(ALCL and ALK-positive large B-cell lymphoma[28]) and sarcoma (IMT,[5] rhabdomyosarcoma,[26] and neuroblastoma[29]). It was not until 2007 that the presence of an ALK fusion was described in lung cancer.[6] This seems to be mainly because EML4-ALK is barely detectable by conventional anti-ALK immunohistochemistry. Considering in reverse, in cases of a tumor that is positive by anti-ALK iAEP immunohistochemistry, but negative by conventional anti-ALK immunohistochemistry, the tumor may have a novel ALK fusion partner, or express wild-type ALK at a modest level. Indeed, in "ALK-negative" IMT cases defined by conventional ALK immunohistochemistry, PPFIBP1-ALK was identified through reassessment for ALK fusions, using anti-ALK iAEP immunohistochemistry.[24] This prompted us to reevaluate other types of solid cancers for ALK fusions. Here, we describe the identification of TPM3-ALK (fusion of tropomyosin 3 and ALK) and EML4-ALK in renal cancer, by anti-ALK iAEP immunohistochemistry.

MATERIALS AND METHODS

Materials

We examined 355 renal tumor tissues from patients who had received surgery in the Cancer Institute Hospital, Japanese Foundation for Cancer Research, Tokyo, between 1994 and 2010. Renal tumors included 255 clear cell renal cell carcinomas (RCCs), 32 papillary RCCs, 34 chromophobe RCCs, 6 collecting duct carcinomas, 10 unclassified RCCs, 6 sarcomatoid RCCs, and 12 other tumors (4 oncocytomas, 3 angiomyolipomas, 1 solitary fibrous tumor, 2 spindle cell sarcomas, 1 desmoplastic sarcoma, and 1 anaplastic carcinoma). Surgically removed tumor specimens were routinely fixed in 20% neutralized formalin and embedded in paraffin for conventional histopathological examination. Immunohistochemical screenings were performed using tissue microarrays. For the 2 cases positive for anti-ALK immunohistochemistry, total RNA was extracted from the corresponding snap-frozen specimen, and purified with the use of an RNeasy Mini kit (Qiagen, Tokyo, Japan). Informed consent was obtained from the patients. The study was approved by the institutional review board of the Japanese Foundation for Cancer Research.

Immunohistochemistry

Formalin-fixed, paraffin-embedded tissue was sliced at a thickness of 4 μm, and the sections were placed on silane-coated slides. For antigen retrieval, the slides were heated for 45 minutes at 102°C in antigen retrieval solution (Nichirei Bioscience, Tokyo). For conventional immunostaining, the slides were incubated at room temperature with primary antibodies: ALK (5A4), vimentin, epithelial membrane antigen (EMA), cytokeratin 7, AE1/AE3, CAM5.2, 34βE12, α-methylacyl-coenzymeA racemase (AMACR), clusters of differentiation 10 (CD10), transcription termination factor 1 (TTF1), renal cell carcinoma marker (RCC Ma), paired box 2 (PAX2), and paired box 8 (PAX8) for 30 minutes. The immune complexes were then detected with polymer reagent (Histofine Simple Stain MAX PO; Nichirei Bioscience, Tokyo, Japan). For the sensitive detection of ALK fusion proteins, the ALK Detection Kit (Nichirei Bioscience), which is based on the iAEP method, was used.

Isolation of ALK Fusions

To obtain complementary DNA (cDNA) fragments corresponding to a novel ALK fusion gene, we used a 5′ rapid amplification of cDNA ends (5′-RACE) method with the SMARTer RACE cDNA Amplification Kit (Clontech, Takara Bio Inc., Shiga, Japan). We followed the manufacturer's instructions, with a minor modification: the ALK2458R primer (5′-GTAGTTGGGGTTGTAGTC GGTCATGATGGT-3′) was used as the gene-specific reverse primer. From the deoxythymidine oligomer–primed cDNA obtained from RNA from case 1, a 385–base pair (bp) cDNA fragment containing the fusion point was specifically amplified with the primers TPM3-705F (5′-AGAGACCCGTGCTGAGTTTGCTG-3′) and ALK3078RR (5′-ATCCAGTTCGTCCTGTTCA GAGC-3′). From case 2, a 454-bp cDNA fragment containing the fusion point was specifically amplified with the primers EML4-72F (5′-GTCAGCTCTTGAGT CACGAGTT-3′) and ALK3078RR. Polymerase chain reaction (PCR) analysis of genomic DNA for TPM3-ALK in case 1 was carried out with a pair of primers flanking the putative fusion point: TPM3-705F (5′-AGA GACCCGTGCTGAGTTTGCTG-3′) and Fusion-RT-AS (5′-TCTTGCCAGCAAAGCAGTAGTTGG-3′). For genomic PCR analysis of EML4-ALK in case 2, we used primers EML4-107F (5′-ATGAAATCACTGTGCTAA AGGCGGCT-3′) and Fusion-RT-AS (5′-TCTTGCCA GCAAAGCAGTAGTTGG-3′).

Fluorescence In Situ Hybridization

Fluorescence in situ hybridization (FISH) analysis of gene fusion was carried out with DNA probes for ALK, TPM3, EML4, and transcription factor E3 (TFE3). Unstained sections (4 μm thick) were subjected to hybridization with an ALK-split probe set (Dako, Tokyo, Japan), TFE3-split probe set (Kreatech, Amsterdam, The Netherlands), or bacterial artificial chromosome (BAC) clone-derived

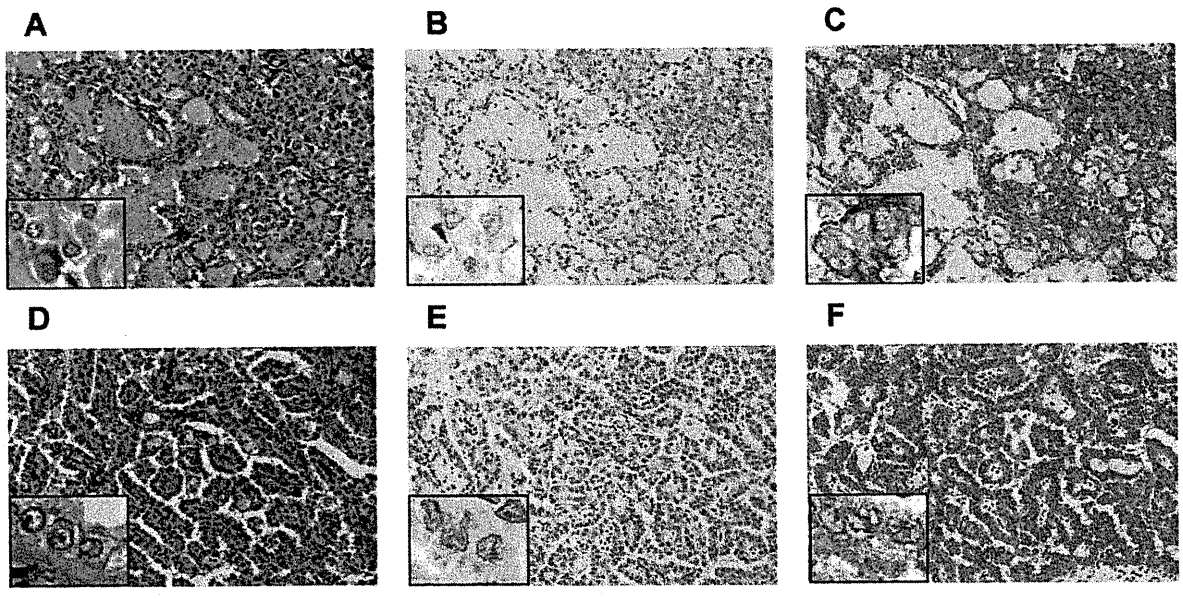

Figure 2. Histopathology of anaplastic lymphoma kinase (ALK)-positive renal cancer. Cuboidal tumor cells showed papillary, tubular, or cribriform growth patterns. The tumor cells had eosinophilic cytoplasm and round to ovoid nuclei. (A) The glandular structures possessed abundant mucin. (D) The tumor comprised a papillary structure of cuboidal or low columnar cells, with eosinophilic cytoplasm and small uniform round to oval nuclei (A,D hematoxylin and eosin stain). The tumor cells were (B) weakly positive and (E) indeterminate for ALK with conventional anti-ALK immunohistochemistry. (C,F) All of the tumor cells were clearly positive for ALK when the iAEP method was used. The staining pattern was diffuse cytoplasmic, with (C) membranous or (F) fine granular accentuation. Figures were taken using the corresponding whole sections (× 10 objective for low power view. × 40 objective for inset). Case 1 (A-C); Case 2 (D-F).

probes for ALK (RP11-984I21, RP11-62B19, RP11-701P18), TPM3 (RP11-809B24), and EML4 (RP11-996L7). Hybridized slides were then stained with 4′,6-diamidino-2-phenylindole and examined using a fluorescence microscope BX51 (Olympus, Tokyo, Japan).

Mutation Analyses for MET

A 1007-bp cDNA fragment containing the MET kinase domain was amplified using the primers MET-3186F (5′-GTCCATTACTGCAAAATACTGTCC-3′) and MET-4193R (5′-CACCTCATCATCAGCGTTATC-3′). The PCR product was sequenced after subcloning.

RESULTS

Identification of ALK Fusions in RCC Samples

Sections of tissue microarray were immunostained for ALK by the iAEP method, resulting in the detection of 2 positive cases (case 1, Fig. 2A-C; case 2, Fig. 2D-F). The positive results were also confirmed using corresponding whole histopathological sections, in which all of the tumor cells stained for ALK as other ALK-positive cancers usually do. We carried out 5′-RACE assays to determine whether these cases expressed ALK fusion or full-length ALK (mutated or unmutated). We isolated a cDNA fragment containing the exon 8 of *TPM3* fused in-frame to the exon 20 of *ALK* (Fig. 3A) in case 1, and the exon 2 of *EML4* fused to the exon 20 of *ALK* in case 2 (Fig. 3B). This EML4-ALK is called variant 5 (E2;A20) in lung cancer.[30] Reverse transcription PCR (RT-PCR) assays designed for the *TPM3-ALK* or E2;A20 successfully amplified cDNAs containing the fusion points (Fig. 3C,D). To confirm the genomic rearrangement, we performed FISH assays (Fig. 4) and genomic PCR (data not shown) for each fusion. All our results were consistent with the presence of t(1;2)(p21;p23)/*TPM3-ALK* in case 1, or inv(2)(p21p23)/E2;A20 in case 2. No other cases were positive for ALK by iAEP immunohistochemistry. All 355 cases were further examined by ALK-split FISH assay. In 12 of the cases, FISH was unsuccessful and not evaluable. In the other cases, the results were identical to those obtained by anti-ALK iAEP immunohistochemistry.

Case Presentation

Case 1

The patient was a 36-year-old woman who had a complaint suggestive of pyelonephritis. Magnetic resonance imaging and computed tomography showed a mass (4.0 cm × 4.0 cm × 3.5 cm) in the left kidney. No metastatic lesions or lymph node enlargements were identified. The patient had no past medical history of malignancy.

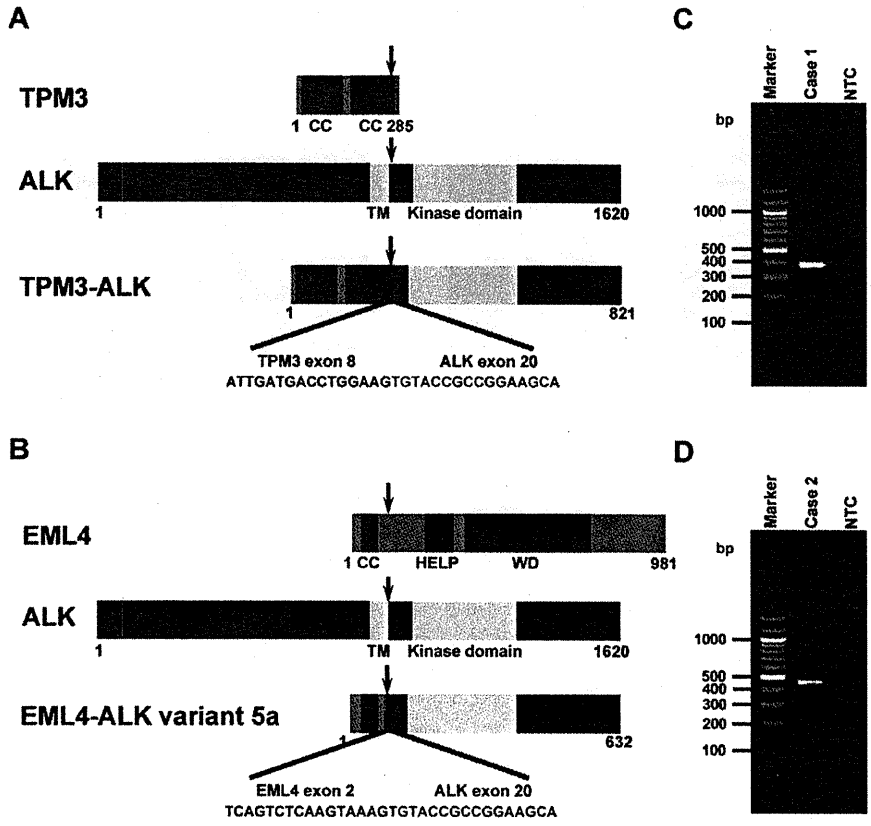

Figure 3. Identification of anaplastic lymphoma kinase (ALK) fusions. Tropomyosin 3 (TPM3) harbors 2 coiled-coil domains. (A) Case 1. A chromosome translocation generates a fusion protein in which the 2 coiled-coil domains of TPM3 and the intracellular region of ALK (containing the tyrosine kinase domain) are conserved. (B) Nucleotide sequencing of the polymerase chain reaction (PCR) products in case 2 revealed that exon 2 of echinoderm microtubule-associated protein like 4 (EML4), comprising a coiled-coil domain, was fused to exon 20 of ALK, generating the variant 5 complementary DNA (cDNA). In TPM3 and EML4 fusions, the region containing the coiled-coil domain is fused to the kinase domain of ALK. Numbers indicate amino acid positions of each protein. Arrow indicates the chromosomal breakpoint. The cDNA fragments of 385 base pairs (bp) and 454 bp were obtained by reverse transcription PCR, corresponding to (C) *TPM3-ALK* and (D) *EML4-ALK* variant 5, respectively. The left lane ("Marker") contains DNA size standards (100-bp ladder). CC indicates coiled-coil domain; HELP, hydrophobic echinoderm microtubule-associated protein; NTC, no-template control; TM, transmembrane domain; WD, WD repeats.

She underwent a translumbar left-radical nephrectomy and is currently alive and well without evidence of disease at 2 years of follow-up.

Case 2

A 53-year-old woman was found incidentally to have microscopic hematuria by medical check-up. Ultrasonography and magnetic resonance imaging showed a change in the left kidney, but the diagnosis was indefinite at that time. One year later, adenocarcinoma cells were detected by urinary cytology, and computed tomography revealed an isodence left renal mass (2.5 cm × 2.5 cm × 2.3 cm). The patient underwent a translumbar left-radical nephrectomy. She is currently alive and well at 7 years after surgery.

The patients had no episodes or family history indicative of sickle cell trait. To the best of our knowledge, there is no reported case of (genetically) Japanese individuals with sickle cell trait/disease.

Histopathological Examinations

The 2 ALK-positive renal cancers were papillary subtype and unclassified (with mixed features of papillary, mucinous cribriform, and solid patterns with rhabdoid cells). They comprised 2.3% of non–clear cell RCCs (2 of 88) and 3.7% of non–clear cell and nonchromophobe RCCs (2 of 54).

Case 1

Histologically, tumor cells were composed of papillary, tubular, or cribriform growth of cuboidal cells with

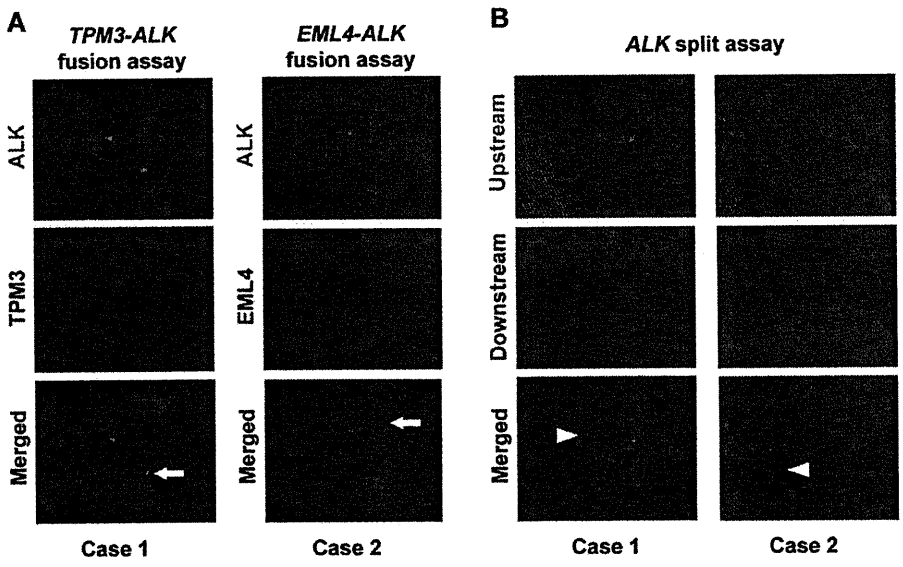

Figure 4. Fluorescence in situ hybridization analyses for *TPM3-ALK* (tropomyosin 3 fusion with anaplastic lymphoma kinase) and *EML4-ALK* (echinoderm microtubule-associated protein like 4 fusion with ALK). (A) In the *TPM3-ALK* and *EML4-ALK* fusion assays, the fusion genes are indicated by arrows. (B) The same clinical specimens as in (A) were subjected to fluorescence in situ hybridization analysis with differentially labeled probes for the upstream (green) or downstream (red) to the ALK breakpoint. In each case, the absence of 1 upstream signal indicated ALK rearrangement. Arrowhead indicates the rearranged ALK. The color of fluorescence for the bacterial artificial chromosome clones and the case numbers are indicated. Nuclei are stained blue with 4′,6-diamidino-2-phenylindole.

eosinophilic cytoplasm. The cribriform morphology consisted of tubular structures with flattened epithelial cells, compressed by mucinous pool and inter- or intracytoplasmic vacuoles. Solid sheets of tumor cells with occasional deeply eosinophilic intracytoplasmic inclusions and eccentric nuclei, resulting in rhabdoid features, were focally identified. Nuclei were round to ovoid, and the nuclear size was basically uniform. Irregular nuclear membranes and nuclear grooves were occasionally observed. Mitotic figures were scant. The background stroma in the tumor area possessed abundant mucin. Frequent deposition of psammoma bodies and infiltration of numerous foamy macrophages were also seen. A large amount of mucinous matrix was highlighted with Alcian blue stain. These histological features resembled the mucinous cribriform pattern frequently observed in ALK-positive lung adenocarcinoma,[18,31] and also a representative case of unclassified RCC by Lopez-Beltran et al,[32] favoring a diagnosis of unclassified RCC. Immunohistochemically, neoplastic cells showed a diffuse and strong positivity for ALK (iAEP), vimentin, EMA, cytokeratin 7, AE1/AE3, cytokeratin CAM5.2, and cytokeratin 34βE12, and focally staining for PAX2, PAX8, AMACR, and CD10. TTF1 and RCC Ma were completely negative. Intracytoplasmic inclusions corresponded to aggregates of intermediate filaments of vimentin. The ALK-staining pattern appeared to be accentuated around the cell membrane of rhabdoid cells. The MIB1 (mindbomb homolog 1) labeling index was less than 1%.

Case 2

Histologically, the tumor consisted of papillary configuration of cuboidal or low columnar cells, with eosinophilic cytoplasm and small uniform round to oval nuclei. A clear cell change was focally seen. Nuclei showed a round to oval shape, and nuclear grooves were frequently observed. The size variation of nuclei was minimal, and the irregularity of the nuclear membrane was evident. Nuclear pseudoinclusions were seldom seen. Small nucleoli were occasionally identified, but mitoses were absent. The fibrovascular cores of papillary architecture contained numerous psammoma bodies and foamy macrophages. In addition, glandular lumens of tumor cells focally contained myxoid materials. These findings morphologically corresponded to papillary RCC, but did not fit to types 1 and 2 by the classification of Delahunt and Eble.[33] In contrast, the features resembled papillary RCC, type 2A, described by Yang et al.[34] Alcian blue stain highlighted a small amount of stromal-type mucin. Upon immunohistochemical analysis, neoplastic cells were diffusely and

strongly positive for ALK (iAEP), vimentin, EMA, cytokeratin 7, AE1/AE3, cytokeratin CAM5.2, cytokeratin 34βE12, and AMACR, and focally positive for PAX2 and PAX8, but negative for TTF1, CD10, and RCC Ma.

Examinations of Other Gene Aberrations

For *MET*, a cDNA fragment with the predicted size was obtained by RT-PCR in case 1. In case 2, no products were identified, indicating that the tumor of the patient did not express *MET*. No mutations were identified in case 1 by sequencing. TFE3 split signals were not observed in either of the 2 cases by FISH.

DISCUSSION

Recently, 2 independent groups have reported vinculin-ALK (VCL-ALK) in renal cancer (Table 1).[35,36] These findings broaden the spectrum of ALK fusion–positive tumors. Interestingly, the 2 patients described in the reports share several uncommon backgrounds for renal cancer: very early onset (6- and 16-year-old boys), a history of sickle cell trait, and uncommon histopathological subtypes (medullary subtype and indeterminate subtype with mixed features of medullary, chromophobe, and transitional cell subtypes). In this study, we screened 355 renal tumors, including 343 RCCs, and identified ALK fusions in 2 RCCs. Significantly, we identified ALK fusions in adult patients (36- and 53-year-old females) without sickle cell trait. This finding will provide a key to ALK inhibitor therapy for more common renal cancers.

RCC associated with *TFE3* gene fusions is already a distinctive entity in the World Health Organization classification,[37,38] and *MET* mutation has been described in 13% of sporadic papillary RCCs.[39] In the present study, we identified neither *MET* nor *TFE3* aberrations in our ALK-positive renal cancer cases. *ALK* rearrangements are recognized as almost mutually exclusive to other mutations such as *EGFR* (epidermal growth factor receptor) and *KRAS* (v-Ki-ras2 Kirsten rat sarcoma viral oncogene) in lung cancer.[6,40] All of the tumor cells in the 2 ALK-positive renal cancers observed by immunohistochemistry expressed ALK fusion protein, suggesting that all tumor cells harbor one or more *ALK* fusion genes. Therefore, as well as other ALK-positive tumors, *ALK* rearrangement in renal cancer probably occurs at a very early phase of carcinogenesis, and is likely to be a driver mutation and mutually exclusive to other driver mutations. As in the case of ALK-positive ALCL, ALK-positive renal cancer will be a distinct molecular pathological entity.

TPM3-ALK was first identified in ALCL in 1999,[41] and subsequently found in IMT in 2000.[5] Therefore, RCC is the third type of cancer that may harbor TPM3-ALK. The organ distribution of EML4-ALK is somewhat controversial. Since its discovery, EML4-ALK has been reported to be identified in lung, breast, and colon cancers. Many research groups have reported the presence of EML4-ALK in a small subset of lung adenocarcinomas (2%-10%). Interestingly, a group in the United States reported the presence of EML4-ALK in breast (5 of 209) and colorectal (2 of 83) cancers, identified by RT-PCR optimized for variants 1, 2, and 3, without showing histopathological evidence.[42] In contrast, 2 Japanese groups examined these cancers (90 breast and 96 colon cancers by RT-PCR for EML4-ALK variants 1 and 2, and 48 breast and 50 colon cancers by multiplex RT-PCR for all possible fusions), but detected no positive cases.[30,43] One possible reason for this discrepancy may be differences in ethnicity. In the present study, we showed histopathological features of the 2 ALK-positive renal cancers. In addition to morphology, the positivity of PAX2 and PAX8 and the negativity of TTF1 strongly indicated that the ALK-positive cancers of the present cases were primary RCCs, and not metastatic lesions of ALK-positive lung cancer.

The oncogenic activities of TPM3-ALK and EML4-ALK have previously been documented,[30,44] and therefore we did not demonstrate them in the present study. As in the case of other ALK-positive tumors, ALK-positive renal cancer is a promising candidate disease for ALK inhibitor therapy. In the present study, we screened surgically removable cases; the prognoses for the 2 ALK-positive patients were good, without recurrence. To realize the full potential of ALK inhibitors in renal cancers, it is important to identify the detailed clinicopathological features of ALK-positive cases, especially those of advanced or recurrent cases, by large-scale screening. For this purpose, anti-ALK immunohistochemistry can most readily be carried out as a primary screening tool. However, caution is needed; the screening immunohistochemical assay should be appropriately sensitive, because our present findings indicate that renal cancer involves EML4-ALK, which is barely detectable by conventional immunohistochemistry methods.[13,45]

Is morphology a clue to the presence of ALK fusion in renal cancers? Almost all ALK-positive lung cancers are adenocarcinomas, and more frequently show mucinous cribriform patterns and signet-ring cells than do ALK-negative adenocarcinomas.[18,31,46] ALK fusion is probably very rare in clear cell RCC, which is the most common

Table 1. ALK-Positive Renal Cancers: Present Cases and Review of Literature

Characteristic	VCL-ALK (Debelenko et al[36])	VCL-ALK (Marino-Enriquez et al[35])	TPM3-ALK (Case 1)	EML4-ALK (Case 2)
Age, y	16	6	36	53
Sex	Male	Male	Female	Female
Ethnicity	African American	African American	Japanese	Japanese
Past history	Sickle cell trait	Sickle cell trait	Tuberculosis (22 y old)	Pleomorphic adenoma (50 y old)
Karyotype	Abnormal complex karyotype	46,XY,t(2;10)(p23;q22), add(14)(p11)	Not examined	Not examined
Symptom	Right flank pain, gross hematuria	Intermittent periumbilical pain, hematuria	Pyelonephritis	Microscopic hematuria
Stage	Stage III	Stage I	Stage I	Stage I
Follow-up	9 mo, alive. No evidence of disease	21 mo, alive. No evidence of disease	2 y, alive. No evidence of disease	3 y, alive. No evidence of disease
Gross findings	6.5-cm irregularly shaped solid tumor mass with infiltrative borders centered in the right renal medulla	4.5-cm irregularly spherical mass with lobulated, fleshy light tan appearance centered in the medulla	4.0 cm × 4.0 cm × 3.5 cm irregularly shaped solid tumor with expansive borders centered in the cortex	Double cancer. A: 2.5 cm × 2.5 cm ×2.3 cm solid yellow tumor in the cortex of the left intermediate pole. B: 0.6-cm yellow mass in the cortex of the left inferior pole
Microscopic findings	Diffuse sheet-like pattern; round, oval, and polygonal tumor cells; eosinophilic cytoplasm; moderately polymorphic and vesicular nuclei	Solid growth pattern; spindle-shaped cells with large vesicular nuclei; clear coarse chromatin and abundant eosinophilic cytoplasm	Papillary, tubular, or cribriform growth of cuboidal cells with eosinophilic cytoplasm. Nuclei round to ovoid; nuclear size basically uniform	A: Papillary structure of cuboidal or low columnar cells with eosinophilic cytoplasm and small uniform round to oval nuclei. B: Clear cell
Immunohistochemistry	Positive: AE1/AE3, CAM5.2, CK7, EMA, INI1, TFE3. Negative: CD10, S100, HMB45, WT1	Positive: AE1/AE3, CAM5.2, EMA	Positive: ALK, vimentin, EMA, cytokeratin 7, AE1/AE3, CAM5.2, 34βE12, AMACR (focal), CD10 (focal), PAX2 (focal), PAX8 (focal). Negative: TTF1, RCC Ma	A: Positive: ALK, vimentin, EMA, cytokeratin 7, AE1/AE3, CAM5.2, 34βE12, AMACR, PAX2 (focal), PAX8 (focal). Negative: CD10, TTF1, RCC Ma
Diagnosis	Renal cell carcinoma, indeterminate subtype (medullary, chromophobe, transitional cell carcinoma mixed)	Renal medullary carcinoma	Renal cell carcinoma, unclassified	A: Papillary renal cell carcinoma, type 2A. B: Clear cell renal cell carcinoma

ALK indicates anaplastic lymphoma kinase; EML4, echinoderm microtubule–associated protein like 4; TPM3, tropomyosin 3; VCL, vinculin.

subtype of renal cancer; 2 previously reported cases with VCL-ALK were not clear cell RCC,[35,36] and we identified no ALK-positive cases in 255 clear cell RCCs in this study. Interestingly, case 1 showed a mucinous cribriform pattern. This may be a characteristic feature of ALK-positive carcinomas, universally applicable to carcinomas of various organs. Further study with a larger number of cases is warranted.

Molecular-targeted therapy of advanced renal cancers is starting to realize its full potential. However, complete remission is rarely achieved, because no agent targets a key molecule associated with "oncogene addiction" of renal cancer. In this context, ALK fusion constitutes a promising advance in renal cancers, as has previously been demonstrated with various other types of cancer. In the present study, we identified 2 adult cases of ALK-positive renal cancer in patients without uncommon backgrounds. Our findings confirm the potential of ALK inhibitor therapy for RCC. More detailed clinicopathological features of ALK-positive renal cancers, especially at higher clinical stages, are desirable. Hunting the "ALKoma" in various types of carcinomas, as well as in lung and kidney cancer, will provide an answer to these pathological and clinical questions.

FUNDING SOURCES

This work was supported in part by Grants-in-Aid for Scientific Research from the Ministry of Education, Culture, Sports, Science, and Technology of Japan as well as by grants from the Japan Society for the Promotion of Science; the Ministry of Health, Labour, and Welfare of Japan; the Vehicle Racing Commemorative Foundation of Japan; Princess Takamatsu Cancer Research Fund; and the Uehara Memorial Foundation.

CONFLICT OF INTEREST DISCLOSURE

Dr. Takeuchi is a scientific advisor for the anti-ALK iAEP immunohistochemistry kit (ALK Detection Kit, Nichirei Bioscience, Tokyo, Japan). All remaining authors have made no disclosures.

REFERENCES

1. International Agency for Research on Cancer. The GLOBOCAN Project: GLOBOCAN 2008. http://globocan.iarc.fr/. Accessed December 16, 2011.
2. Campbell SC, Novick AC, Bukowski RM. Renal tumors. In: Wein AJ, Kavoussi LR, Novick AC, Partin AW, Peters CA, eds. Campbell-Walsh Urology. 9th ed. Philadelphia, PA: Saunders; 2007: 1567-1637.
3. Morris SW, Kirstein MN, Valentine MB, et al. Fusion of a kinase gene, ALK, to a nucleolar protein gene, NPM, in non-Hodgkin's lymphoma. *Science.* 1994;263:1281-1284.
4. Shiota M, Fujimoto J, Semba T, Satoh H, Yamamoto T, Mori S. Hyperphosphorylation of a novel 80 kDa protein-tyrosine kinase similar to Ltk in a human Ki-1 lymphoma cell line, AMS3. *Oncogene.* 1994;9:1567-1574.
5. Lawrence B, Perez-Atayde A, Hibbard MK, et al. TPM3-ALK and TPM4-ALK oncogenes in inflammatory myofibroblastic tumors. *Am J Pathol.* 2000;157:377-384.
6. Soda M, Choi YL, Enomoto M, et al. Identification of the transforming EML4-ALK fusion gene in non-small-cell lung cancer. *Nature.* 2007;448:561-566.
7. Rikova K, Guo A, Zeng Q, et al. Global survey of phosphotyrosine signaling identifies oncogenic kinases in lung cancer. *Cell.* 2007; 131:1190-1203.
8. Soda M, Takada S, Takeuchi K, et al. A mouse model for EML4-ALK-positive lung cancer. *Proc Natl Acad Sci U S A.* 2008;105: 19893-19897.
9. Kwak EL, Bang YJ, Camidge DR, et al. Anaplastic lymphoma kinase inhibition in non-small-cell lung cancer. *N Engl J Med.* 2010;363:1693-1703.
10. Chihara D, Suzuki R. More on crizotinib. *N Engl J Med.* 2011;364: 776-777.
11. Butrynski JE, D'Adamo DR, Hornick JL, et al. Crizotinib in ALK-rearranged inflammatory myofibroblastic tumor. *N Engl J Med.* 2010;363:1727-1733.
12. Gambacorti-Passerini C, Messa C, Pogliani EM. Crizotinib in anaplastic large-cell lymphoma. *N Engl J Med.* 2011;364:775-776.
13. Takeuchi K, Choi YL, Togashi Y, et al. KIF5B-ALK, a novel fusion oncokinase identified by an immunohistochemistry-based diagnostic system for ALK-positive lung cancer. *Clin Cancer Res.* 2009;15: 3143-3149.
14. Martelli MP, Sozzi G, Hernandez L, et al. EML4-ALK rearrangement in non-small cell lung cancer and non-tumor lung tissues. *Am J Pathol.* 2009;174:661-670.
15. Jokoji R, Yamasaki T, Minami S, et al. Combination of morphological feature analysis and immunohistochemistry is useful for screening of EML4-ALK-positive lung adenocarcinoma. *J Clin Pathol.* 2010;63:1066-1070.
16. Kijima T, Takeuchi K, Tetsumoto S, et al. Favorable response to crizotinib in three patients with echinoderm microtubule-associated protein-like 4-anaplastic lymphoma kinase fusion-type oncogene-positive non-small cell lung cancer. *Cancer Sci.* 2011;102:1602-1604.
17. Kimura H, Nakajima T, Takeuchi K, et al. ALK fusion gene positive lung cancer and 3 cases treated with an inhibitor for ALK kinase activity. *Lung Cancer.* 2012;75:66-72.
18. Yoshida A, Tsuta K, Nakamura H, et al. Comprehensive histologic analysis of ALK-rearranged lung carcinomas. *Am J Surg Pathol.* 2011;35:1226-1234.
19. Yi ES, Boland JM, Maleszewski JJ, et al. Correlation of IHC and FISH for ALK gene rearrangement in non-small cell lung carcinoma: IHC score algorithm for FISH. *J Thorac Oncol.* 2011;6:459-465.
20. Kudo K, Takeuchi K, Tanaka H, et al. Immunohistochemical screening of ALK lung cancer with biopsy specimens of advanced lung cancer. *J Clin Oncol.* 2010;28(suppl): (abstract 10532).
21. Sakairi Y, Nakajima T, Yasufuku K, et al. EML4-ALK fusion gene assessment using metastatic lymph node samples obtained by endobronchial ultrasound-guided transbronchial needle aspiration. *Clin Cancer Res.* 2010;16:4938-4945.
22. Nakajima T, Kimura H, Takeuchi K, et al. Treatment of lung cancer with an ALK Inhibitor after EML4-ALK fusion gene detection using endobronchial ultrasound-guided transbronchial needle aspiration. *J Thorac Oncol.* 2010;5:2041-2043.
23. Takeuchi K, Soda M, Togashi Y, et al. Identification of a novel fusion, SQSTM1-ALK, in ALK-positive large B-cell lymphoma. *Haematologica.* 2011;96:464-467.
24. Takeuchi K, Soda M, Togashi Y, et al. Pulmonary inflammatory myofibroblastic tumor expressing a novel fusion, PPFIBP1-ALK: reappraisal of anti-ALK immunohistochemistry as a tool for novel ALK-fusion identification. *Clin Cancer Res.* 2011;17:3341-3348.
25. Shiota M, Fujimoto J, Takenaga M, et al. Diagnosis of t(2;5)(p23;q35)-associated Ki-1 lymphoma with immunohistochemistry. *Blood.* 1994;84:3648-3652.
26. Pulford K, Lamant L, Morris SW, et al. Detection of anaplastic lymphoma kinase (ALK) and nucleolar protein nucleophosmin (NPM)-ALK proteins in normal and neoplastic cells with the monoclonal antibody ALK1. *Blood.* 1997;89:1394-1404.
27. Shiota M, Nakamura S, Ichinohasama R, et al. Anaplastic large cell lymphomas expressing the novel chimeric protein p80NPM/ALK: a distinct clinicopathologic entity. *Blood.* 1995;86:1954-1960.
28. Delsol G, Lamant L, Mariamé B, et al. A new subtype of large B-cell lymphoma expressing the ALK kinase and lacking the 2; 5 translocation. *Blood.* 1997;89:1483-1490.
29. Lamant L, Pulford K, Bischof D, et al. Expression of the ALK tyrosine kinase gene in neuroblastoma. *Am J Pathol.* 2000;156:1711-1721.
30. Takeuchi K, Choi YL, Soda M, et al. Multiplex reverse transcription-PCR screening for EML4-ALK fusion transcripts. *Clin Cancer Res.* 2008;14:6618-6624.
31. Inamura K, Takeuchi K, Togashi Y, et al. EML4-ALK fusion is linked to histological characteristics in a subset of lung cancers. *J Thorac Oncol.* 2008;3:13-17.
32. Lopez-Beltran A, Carrasco JC, Cheng L, Scarpelli M, Kirkali Z, Montironi R. 2009 update on the classification of renal epithelial tumors in adults. *Int J Urol.* 2009;16:432–443.
33. Delahunt B, Eble JN. Papillary renal cell carcinoma: a clinicopathologic and immunohistochemical study of 105 tumors. *Mod Pathol.* 1997;10:537-544.
34. Yang XJ, Tan MH, Kim HL, et al. A molecular classification of papillary renal cell carcinoma. *Cancer Res.* 2005;65:5628-5637.
35. Mariño-Enríquez A, Ou WB, Weldon CB, Fletcher JA, Pérez-Atayde AR. ALK rearrangement in sickle cell trait-associated renal medullary carcinoma. *Genes Chromosomes Cancer.* 2011;50:146-153.
36. Debelenko LV, Raimondi SC, Daw N, et al. Renal cell carcinoma with novel VCL-ALK fusion: new representative of ALK-associated tumor spectrum. *Mod Pathol.* 2011;24:430-442.
37. Argani P, Ladanyi M. Renal carcinomas associated with Xp11.2 translocations/TFE3 gene fusions. In: Eble J, Sauter G, Epstein J, Sesterhenn I, eds. Pathology and Genetics of Tumours of the Urinary System and Male Genital Organs. Lyon, France: IARC Press; 2004:37-38.
38. Ross H, Argani P. Xp11 translocation renal cell carcinoma. *Pathology.* 2010;42:369-373.

39. Schmidt L, Junker K, Nakaigawa N, et al. Novel mutations of the MET proto-oncogene in papillary renal carcinomas. *Oncogene.* 1999; 18:2343-2350.
40. Inamura K, Takeuchi K, Togashi Y, et al. EML4-ALK lung cancers are characterized by rare other mutations, a TTF-1 cell lineage, an acinar histology, and young onset. *Mod Pathol.* 2009;22:508-515.
41. Lamant L, Dastugue N, Pulford K, Delsol G, Mariamé B. A new fusion gene TPM3-ALK in anaplastic large cell lymphoma created by a (1;2)(q25;p23) translocation. *Blood.* 1999;93: 3088-3095.
42. Lin E, Li L, Guan Y, et al. Exon array profiling detects EML4-ALK fusion in breast, colorectal, and non-small cell lung cancers. *Mol Cancer Res.* 2009;7:1466-1476.
43. Fukuyoshi Y, Inoue H, Kita Y, Utsunomiya T, Ishida T, Mori M. EML4-ALK fusion transcript is not found in gastrointestinal and breast cancers. *Br J Cancer.* 2008;98:1536-1539.
44. Giuriato S, Faumont N, Bousquet E, et al. Development of a conditional bioluminescent transplant model for TPM3-ALK-induced tumorigenesis as a tool to validate ALK-dependent cancer targeted therapy. *Cancer Biol Ther.* 2007;6:1318-1323.
45. Sozzi G, Martelli MP, Conte D, et al. The EML4-ALK transcript but not the fusion protein can be expressed in reactive and neoplastic lymphoid tissues. *Haematologica.* 2009;94:1307-1311.
46. Rodig SJ, Mino-Kenudson M, Dacic S, et al. Unique clinicopathologic features characterize ALK-rearranged lung adenocarcinoma in the western population. *Clin Cancer Res.* 2009;15:5216-5223.

Lung Cancer 75 (2012) 66–72

Contents lists available at ScienceDirect

Lung Cancer

journal homepage: www.elsevier.com/locate/lungcan

ALK fusion gene positive lung cancer and 3 cases treated with an inhibitor for ALK kinase activity

Hideki Kimura[a,*], Takahiro Nakajima[a,d], Kengo Takeuchi[b], Manabu Soda[c], Hiroyuki Mano[c], Toshihiko Iizasa[a], Yukiko Matsui[a], Mitsuru Yoshino[a], Masato Shingyoji[a], Meiji Itakura[a], Makiko Itami[e], Dai Ikebe[e], Sana Yokoi[f], Hajime Kageyama[f], Miki Ohira[g], Akira Nakagawara[h]

[a] Division of Thoracic Diseases, Chiba Cancer Center, Chiba, Japan
[b] Pathology Project for Molecular Targets, Cancer Institute, Japanese Foundation for Cancer Research (JFCR), Koto, Tokyo, Japan
[c] Division of Functional Genomics, Jichi Medical University, Tochigi, Japan
[d] Division of Thoracic Surgery, Toronto General Hospital, University Health Network, Toronto, Canada
[e] Division of Pathology, Chiba Cancer Center, Japan
[f] Cancer Genome Center, Chiba Cancer Center Research Institute, Japan
[g] Laboratory of Cancer Genomics, Chiba Cancer Center Research Institute, Japan
[h] Chiba Cancer Center, Japan

ARTICLE INFO

Article history:
Received 16 October 2010
Received in revised form 24 May 2011
Accepted 30 May 2011

Key words:
ALK
EML4
KIF5B
Fusion gene
Lung cancer
EBUS
TBNA
Crizotinib
ALK inhibitor

ABSTRACT

Background: Anaplastic lymphoma kinase (ALK) fusion gene-positive lung cancer accounts for 4–5% of non-small cell lung carcinoma. A clinical trial of the specific inhibitor of ALK fusion-type tyrosine kinase is currently under way.
Methods: ALK fusion gene products were analyzed immunohistochemically with the materials obtained by surgery or by endobronchial ultrasound-guided transbronchial needle aspiration (EBUS-TBNA). The echinoderm microtubule-associated protein-like 4(EML4)-ALK or kinesin family member 5B (KIF5B)-ALK translocation was confirmed by the reverse transcription polymerase chain reaction (RT-PCR) and fluorescence in situ hybridization (FISH). After eligibility criteria were met and informed consent was obtained, 3 patients were enrolled for the Pfizer Study of Crizotinib (PF02341066), Clinical Trial A8081001, conducted at Seoul National University.
Results: Out of 404 cases, there were 14 of EML4-ALK non-small cell carcinoma (NSCLC) and one KIF5B-ALK NSCLC case (8 men, 7 women; mean age, 61.9 years, range 48–82). Except for 2 light smokers, all patients were non-smokers. All cases were of adenocarcinoma with papillary or acinar subtypes. Three were of stage IA, 5 of stage IIIA, 1 of stage IIIB and 6 of stage IV. Ten patients underwent thoracotomy, 3 received chemotherapy and 2 only best supportive care (BSC). One BSC and 2 chemotherapy cases were enrolled for the clinical trial. Patients with advanced stages who received chemotherapy or best supportive care were younger (54.0 ± 6.3) than those who were surgically treated (65.8 ± 10.1) ($p < 0.05$).
The powerful effect of ALK inhibitor on EML4-ALK NSCLC was observed. Soon after its administration, almost all the multiple bone and lymph node metastases quickly disappeared. Nausea, diarrhea and the persistence of a light image were the main side effects, but they diminished within a few months.
Conclusion: ALK-fusion gene was found in 3.7% (15/404) NSCLC cases and advanced disease with this fusion gene was correlated with younger generation. The ALK inhibitor presented in this study is effective in EML4-ALK NSCLC cases. A further study will be necessary to evaluate the clinical effectiveness of this drug.

1. Introduction

As the mechanisms of carcinogenesis become clearer, the target of cancer treatment is shifting from non-specific cytotoxic agents to specific agents that block key molecular events in the carcinogenesis of malignancy such as EGFR-TKI and anti-HER2 antibody (trastuzumab) [1–3]. Recently, Mano et al. [4–6] reported that a small inversion within chromosome 2p results in the formation of a fusion gene comprising portions of the

* Corresponding author at: Division of Thoracic Diseases, Chiba Cancer Center, 666-2, Nitona-cho, Chuo-ku, 260-8717 Chiba, Japan. Tel.: +81 43 264 5431; fax: +81 43 262 8680.
E-mail address: hkimura@chiba-cc.jp (H. Kimura).

0169-5002/$ – see front matter © 2011 Elsevier Ireland Ltd. All rights reserved.
doi:10.1016/j.lungcan.2011.05.027

echinoderm microtubule-associated protein-like 4 (EML4) gene and the anaplastic lymphoma kinase (ALK) gene in non-small-cell lung cancer. Transgenic mice that express EML4-ALK specifically in lung epithelial cells develop multiple foci of adenocarcinoma in the lung soon after birth, and the oral administration of a specific inhibitor of ALK tyrosine kinase activity eradicated completely the foci of adenocarcinoma. Clinical trials of specific inhibitors of EML4-ALK tumors are currently underway [7–11]. Kwak et al. [11] reported the effect of crizotinib in Clinical Trial A8081001 on the 82 patients with advanced ALK-positive disease. Over a mean treatment duration of 6.4 months, the overall response rate was 57% and the estimated probability of 6-month progression-free survival was 72%. We report 15 cases of ALK fusion gene-positive NSCLC cases and 3 cases in our experience with ALK inhibitor in the Pfizer Study of crizotinib (PF02341066), Clinical Trial A8081001, which was conducted at Seoul National University.

2. Materials and methods

Out of 404 patients who had undergone surgical resection (295 cases) or bronchoscopy (109 cases) in Chiba Cancer Center, Japan, from 2007 to 2009, 15 ALK fusion gene-positive NSCLC patients were initially screened by immunohistochemical procedures. Diagnoses were confirmed by RT-PCR and/or FISH for their molecular translocation.

2.1. ALK fusion protein detection by immunohistochemical methods

The intercalated antibody-enhanced polymer method of Takeuchi et al. [12,13] was used to detect ALK proteins. Formalin-fixed paraffin-embedded tissue was sliced at a thickness of 4 μm and the sections were placed on silane-coated slides. For antigen retrieval, the slides were heated for 40 min at 97 °C in target Retrieval Solution (pH 9.0; Dako). They were then incubated at room temperature, first with Protein Block Serum-free Ready-to-Use solution (Dako) for 10 min, and then with an anti-ALK antibody (5A4, Abcam) for 30 min. To increase the sensitivity of detection, we included an incubation step of 15 min at room temperature with rabbit polyclonal antibodies to mouse immunoglobulin (Dako). The immune complexes were then detected with the dextran polymer reagent and an AutoStainer instrument (Dako).

2.2. Confirmation of EML4-ALK fusion gene by RT-PCR and FISH

We confirmed the existence of ALK fusion gene expression by fluorescence in situ hybridization (FISH) and/or by the reverse transcription-polymerase chain reaction (RT-PCR).

2.3. Fluorescence in situ hybridization (FISH)

An EML4-ALK fusion assay was performed [10–12]. Unstained sections were processed with a Histology FISH Accessory Kit (Dako), subjected to hybridization with fluorescence-labeled bacterial artificial chromosome clone probes for EML4 and ALK (self-produced probes; EML4: RP11-996L7, ALK: RP11-984I21 and RP11-62B19), stained with 4,6-diamidino-2-phenylindole, and examined with a fluorescence microscope (BX51; Olympus). The FISH positivity criteria specified "over 50% cancer cells" for EBUS-TBNA samples.

2.4. Reverse transcription-polymerase chain reaction (RT-PCR)

The multiplex PCR method proposed by the Japanese ALK lung cancer study group (ALCAS) was used to confirm the expression of ALK fusion gene [4–6].

Table 1
Characteristics of ALK fusion gene positive lung cancer patients.

Patient no	Sex	Age	SI	Histology	Variant	p Stage	Therapy	Recurrence	Distant meta	Survival (M)	Prognosis	ALK inhibitor case no
1	f	64	0	Ad: papillary	3	IIIA	Surgery	Positive	Bone, brain	21	Dead	
2	m	82	0	Ad: solid	2	IIIA	Surgery	Positive	Ascites	36	Alive	
3	f	68	0	Ad: papillary	3	IIIB	Surgery	Positive	Brain	34	Alive	
4	f	60	0	Ad: solid	3	IIIA	Surgery	Negative	None	29	Alive	
5	m	73	0	Ad: acinar	3	IA	Surgery	Negative	None	21	Alive	
6	m	66	0	Ad: papillary	KIF5B	IA	Surgery	Negative	None	15	Alive	
7	m	56	300	Ad: papillary	1	IA	Surgery	Negative	None	13	Alive	
8	m	46	0	Ad: acinar	5	IIIA	Surgery	Negative	None	22	Alive	
9	m	71	0	Ad: papillary	1	IIIA	Surgery	Negative		17	Alive	
10	f	73	0	Ad: acinar	1	IV	Surgery	Negative		14	Alive	
11	m	55	100	Ad: muc+	3	IV	BSC		Bone, brain	5	Dead	
12	m	48	0	Ad: muc+	1	IV	Chemo		Bone, brain	29	Dead	Case 1
13	f	49	0	Ad: muc+	3	IV	BSC		Bone, brain	15	Alive	Case 2
14	f	54	0	Ad: muc+	1	IV	Chemo		Bone, brain, pul	22	Alive	Case 3
15	f	64	0	Ad: acinar	3	IV	Chemo		Pul	2	Alive	

SI, smoking index; f, female; m, male; Ad, adenocarcinoma; muc+, mucin production; Distant meta, at the recurrence (surgery group) at the diagnosis (non-surgery group); pul, pulmonary metastasis; Case 1 was already reported by Nakajima et al. [16].

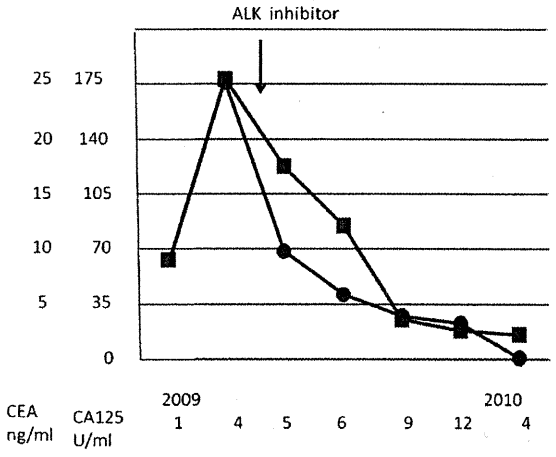

Fig. 1. Changes of tumor markers before and during the treatment with ALK inhibitor (Case 1) CEA (■), CA125 (●). Marked reduction of tumor markers was observed.

Total RNA was isolated from EBUS-TBNA or surgical samples using AllPrep DNA/RNA Mini Kit (Qiagen) and was reverse-transcribed into single strand cDNA using a High Capacity RNA-to-cDNA Kit (Applied Biosystems). To detect a fusion cDNA derived from EML4 or KIF5B and ALK, PCR analysis was performed with the AmpliTaq Gold PCR Master Mix (Applied Biosystems), the forward primers derived from EML4, EA-F-cDNA-S (5′-GTGCAGTGTTTAGCATTCTTGGGG-3′), EA-F-2-g-S (5′-AGCTACATCACACACCTTGACTGG-3′), EA-F-cDNA-v3-S-2 (5′-TACCAGTGCTGTCTCAATTGCAGG-3″) and EA-W-cDNA-in-S (5′-GCTTTCCCCGCAAGATGGACGG-3′) and the forward primers derived from KIF5B, KA-F-cDNA-S-e24 (5′-CAGCTGAGAGAGTGAAAGCTTTGG-3′), KA-F-cDNA-S-e17 (5′-GACAGTTGGAGGAATCTGTCGATG-3′), KA-F-cDNA-S-e11 (5′-ATCCTGCGGAACACTATTCAGTGG-3′), and KA-cDNA-S-e2 (5′-TCAAGCACATCTCAAGAGCAAGTG-3′) and the reverse primer derived from ALK, EA-F-cDNA-A (5′-TCTTGCCAGCAAAG-CAGTAGTTGG-3′). PCR products were purified from gel bands using QIAquick Gel Extraction Kit (Qiagen) and confirmed by direct sequencing analysis.

2.5. Enrolment of patients for the Clinical Trial A8081001

Informed consent was obtained from each patient to be enrolled for the study [10]. Eligibility criteria for the enrolment of ALK translocation positive patients into the ALK TKI PI Trial were as required by the Committee of Clinical Trials A8081001.

3. Results

There were 15 ALK fusion gene-positive cases which were screened immunohistochemically and confirmed by RT-PCR and FISH [14,15]. Eight patients were men and 7 women, of mean age

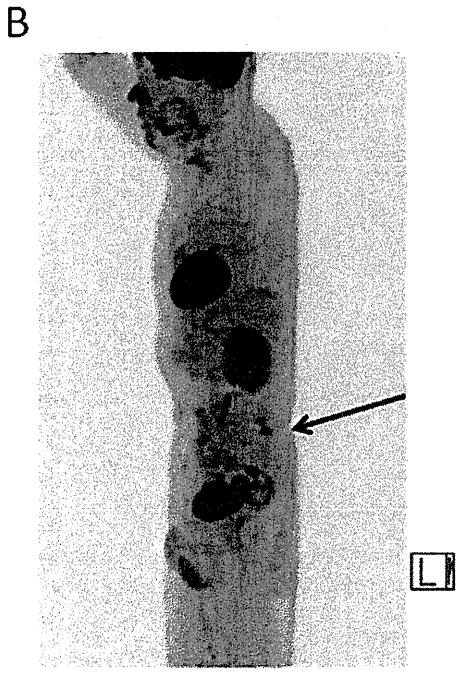

Fig. 2. FDG-PET scan of Case 1 performed at the same time (09/28/2009) as the previously reported Fig. 1D (Nakajima et al. [16]) shows bone metastasis of the left vertebral arch of L5 (arrow) in a sagittal view.

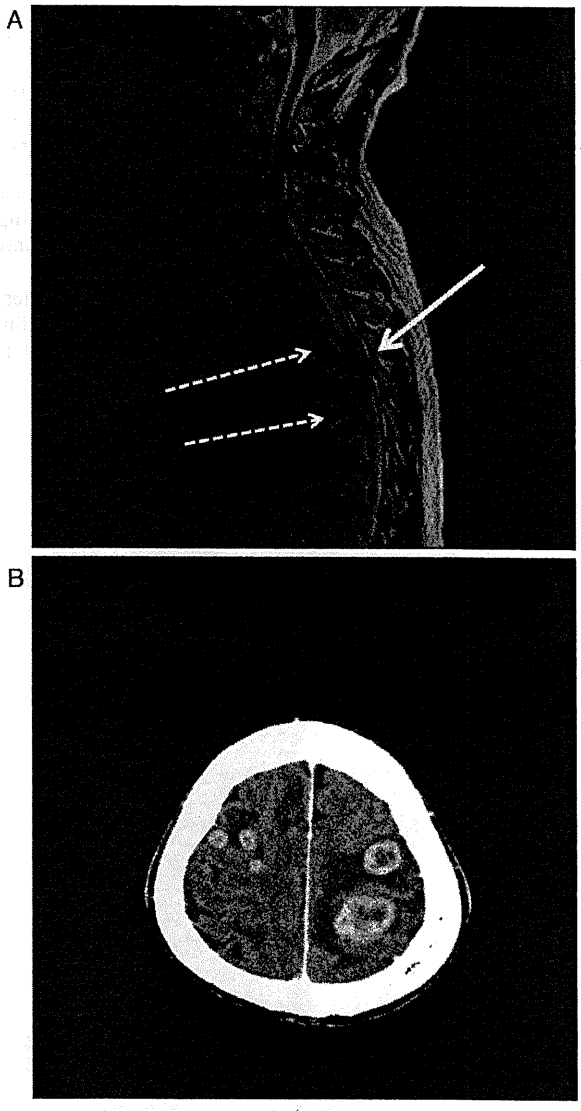

Fig. 3. MRI (Case 1) of the spinal cord on 04/05/2010 shows the metastases to the spinal cord (straight allow) and the spinal column (Th 4,6 dotted allow). B. CT scan (Case 1) of the brain on 04/05/2010 shows multiple brain metastases.

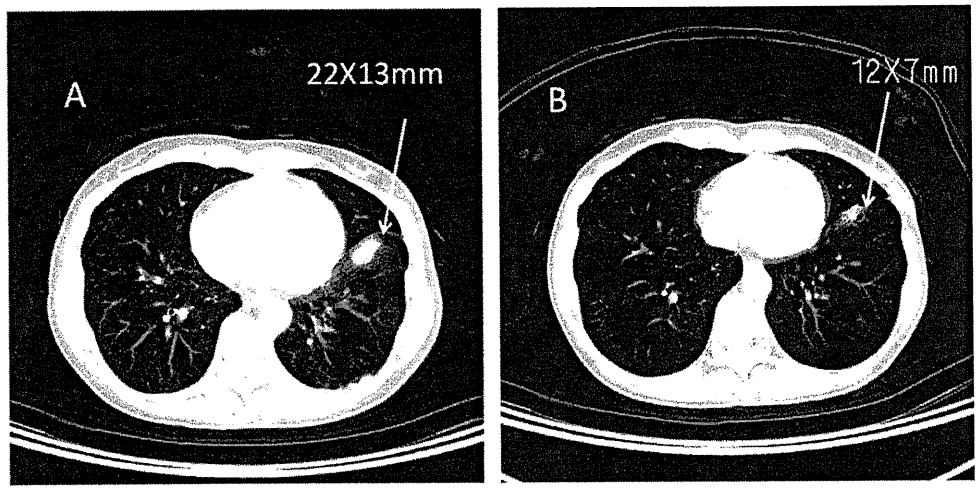

Fig. 4. CT scan (Case 2): A, 07/22/2009 (before ALK inhibitor) and B, 09/02/2009 (5 weeks after the initiation of the therapy). Left S8 tumor (arrow) decreased in size from 22X13 mm to 12X7 mm (PR).

61.9 years (range 48–82). Most were non-smokers, but 2 smoked lightly (Table 1). All tumors were adenocarcinomas with a papillary pattern predominant (5 cases), an acinar pattern predominant (3 cases), with mucin production (4 cases), etc. There were fourteen cases of fusion with EML4 and one KIF5B gene. There were 7 variant 3, 5 variant 1, and 1 each of variants 2 and 5. There were 3 stage IA, 5 stage IIIA, 1 stage IIIB and 6 stage IV cases. Ten cases were diagnosed after surgical resection, and 5, by tissue samples obtained with EBUS-TBNA. Ten cases underwent thoracotomy, 3 cases, chemotherapy, and 2 cases, only best supportive care. Of 5 cases diagnosed by EBUS-TBNA, 2 cases receiving chemotherapy and one receiving best supportive care were enrolled for the clinical trial. The mean age of the surgically treated group was 65.8 ± 10.1, and that of chemotherapy and BSC group was 54.0 ± 6.3. The difference was found by Student's t test to be statistically significant ($p < 0.05$), indicating that younger patients tend to have advanced cancer.

Out of 10 surgically treated cases, seven survived without a sign of recurrence, 3 had recurrence in both bone and brain tissue, and one died of bone and lymph node metastasis.

3.1. Case 1

Case 1 has already been reported in a case report (Nakajima et al.) [16] but without precise descriptions of the response to crizotinib, the adverse effects, the pattern of recurrence or the metastatic

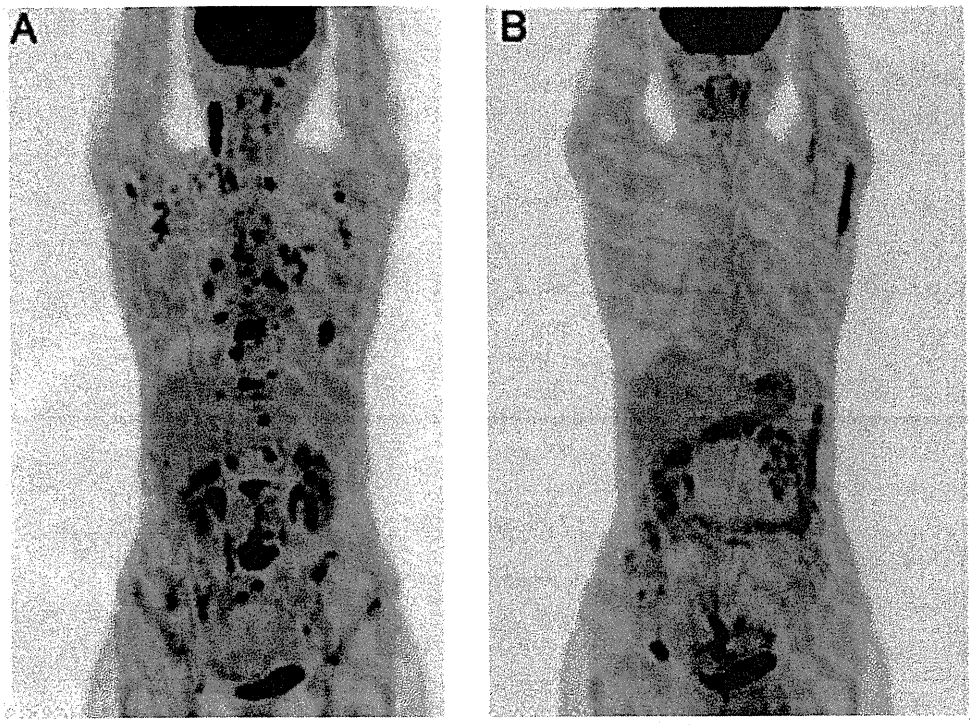

Fig. 5. FDG-PET scan (Case 2): A, 07/22/2009 (before ALK inhibitor) and B, 03/10/2010 FDG-PET scan shows marked reduction of accumulation in multiple bone and lymph node metastases 7 months after the initiation of the treatment.

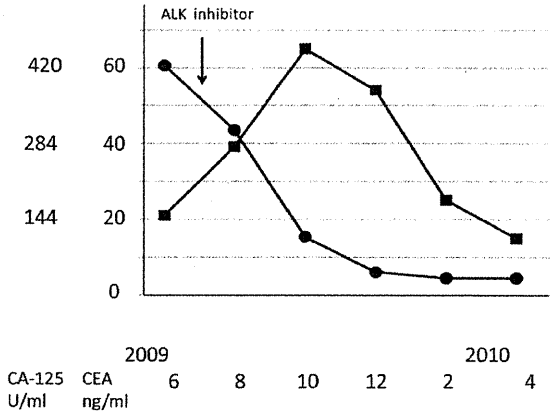

Fig. 6. Changes of tumor markers before and during the treatment with ALK inhibitor in case 2. CA125 (●) gradually decreased along with the treatment, but CEA (■) increased soon after the initiation of the therapy. The value of CEA then gradually decreased to 15.2 ng/ml in April 2010 (after 10 months).

Fig. 7. Brain MRI of case 2 on 7/30/2010 showing multiple metastases.

tumor lesions. Such descriptions may contribute to a better understanding of the other cases, and so case 1 is described briefly below.

A 48-year-old non-smoking male patient had lung adenocarcinoma in the right lower lobe and multiple bone and lymph node metastases (T3N2M1 stage IV) at his first medical examination in November 2007. After several courses of chemotherapy, the patient was enrolled in a trial of crizotinib (PF02341066) from May 5th 2009 at Seoul National University, in which the drug was orally administered at 500 mg/day.

The effect of ALK inhibitor appeared rapidly. The patient's dyspnea improved within one week after drug administration. PS improved from 2 to 0 and a marked reduction in the tumor markers was observed (Fig. 1). Within 3 months after the start of therapy, almost all metastases disappeared except for those at the left vertebral arch of L5 (Fig. 2, arrow). The patient had severe adverse effects: diarrhea, nausea and persistence of light images started soon after the administration of the drug, but these gradually diminished over a 3-week period.

The control of the primary and metastatic tumors continued for 11 months until the patient visited Seoul University in April 2010, when he was hospitalized for paralysis of the lower extremities. MRI revealed spinal column (Th4-6) and spinal cord metastases (Fig. 3A). Soon after his hospitalization in our Cancer Center in April 2010, multiple brain metastases (Fig. 3B) were found, so the drug administration was stopped and he was transferred to a palliative care unit.

Fig. 8. FDG-PET scan: A, 09/08/2009 (before ALK inhibitor) and B, 07/05/2010 FDG-PET scan follow-up for 10 months indicated complete control of primary and distant metastases in case 3.

3.2. Case 2

A 49-year-old woman, a non-smoker with no history of illness, PS0, was introduced to the Orthopedics Department of our Center in April 2009 for back pain and multiple osteoplastic changes in the bones. Systematic examination revealed an abnormal shadow 22X13 mm in size in the left lower lobe (Fig. 4A). Bronchoscopy and a PET scan indicated left S8 adenocarcinoma with cervical, axial, mediastinal, hilar, pancreatic and retroperitoneal lymph node metastases, as well as cranial, thoracic (Th1-12), lumbar (L1-5), rib (1–12) pelvis, humerus, and femur metastases (Fig. 5A).

She refused any therapy except for best supportive care. One month after the examination, an additional immunohistochemical examination for EML4-ALK fusion protein was performed, and found to be positive. The presence of mRNA for EML4-ALK gene was also confirmed by RT-PCR and FISH from the mediastinal #4R lymph nodes obtained with EBUS-TBNA, which was performed 2 months later. EGFR mutation was negative, but the direct sequence of the EML4-ALK mRNA indicated that the translocation was variant 3 [9]. She decided to be enrolled to the crizotinib study (PF02341066) at a dosage of 500 mg/day at Seoul National University from July 2009.

She had nausea, diarrhea and light image persistence as in case 1, but her gastrointestinal symptoms were severer than those in case 1. Two weeks after the administration of ALK inhibitor, her back pain disappeared. A PET scan performed 5 weeks after the initiation of the therapy showed marked reduction of bone and lymph node metastases, and the primary tumor had decreased in size from 22X13 mm to 12X7 mm (Fig. 4A and B). Also, the SUV max dropped from 10.7 to 2.42. Changes of tumor markers were not parallel with the clinical course since the measured value of CA-125 dropped from 424 to 107 U/ml, but that of CEA increased from 21.5 to 65.4 ng/ml 4 months later. The value of CEA then gradually decreased to 15.2 ng/ml in April 2010 (10 months after that: Fig. 6). The PET scan conducted after 7 months indicated a partial response to multiple bone and lymph node metastases (Fig. 5B). The patient continued to take the drug until the end of July 2010, when brain metastases (Fig. 7) were found.

3.3. Case 3

A fifty-four-year-old woman, also a non-smoker, PS0, visited a doctor because of back pain in August 2008. Chest X-ray and CT scan showed an S3 59X22 mm tumor in the right upper lobe, combined with #4R, #2R mediastinal lymph nodes and intrapulmonary metastases. The tumor had invaded the SVC and the azygos vein. She had undergone bronchoscopy and EBUS-TBNA in October 2008. A diagnosis of lung adenocarcinoma was obtained with TBNA samples from #7 lymph nodes. Bone scans indicated cranial, costal, vertebral, scapular, pelvic and femoral metastases (T4N2M1 stage IV). She received 2 courses of CBDCA + GEM (1000 mg/m^2) and 7 courses of docetaxel (TXTL: 60 mg/m^2) from November 2008 to June 2009, but the effect was minimal.

EML4-ALK fusion gene was suggested immunohistochemically in August 2009 and confirmed by RT-PCR obtained by EBUS-TBNA samples from the primary tumor in September 2009. She was enrolled for the clinical trial from November 2009 with an oral administration of crizotinib 500 mg/day. Dyspnea and cough were alleviated within 2 weeks, and she complained of severe diarrhea, nausea, vomiting, light image persistence and perceived changes of taste. A PET scan one month after the start of the treatment demonstrated complete disappearance of the primary tumor as well as all the metastases except for a bone metastasis to the right 8th rib. A PET scan follow-up 8 months later indicated complete control of primary and metastatic tumors (Fig. 8A and B). CEA declined slowly from 1764 ng/ml to 79 ng/ml 6 months after the start of administration (Fig. 9). The patient had 12 brain metastases from 5 mm^3 to 309 mm^3 in volume and underwent gamma knife irradiation in August 2009, 2 months before the start of ALK inhibitor treatment. The irradiated field still showed little change for 5 months, but small new lesions appeared in the left occipital area 6 months after the start of the trial. Brain metastases grew very slowly, so we have maintained our observation until October 2010.

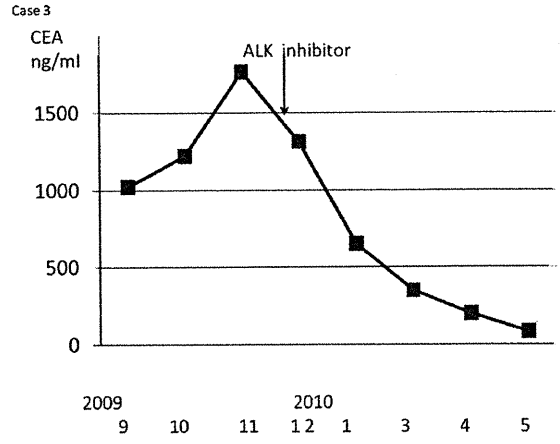

Fig. 9. CEA (■) declined slowly from 1764 ng/ml to 79 ng/ml 6 months after the start of the therapy in case 3.

4. Discussion

Above, we have reported the far-reaching effects of an ALK inhibitor on *EML4-ALK*-positive lung cancer patients. Soon after the administration of crizotinib, almost all metastases to bone and lymph nodes rapidly disappeared, followed by a marked reduction in the level of tumor markers in the sera. These observations clearly support the pivotal role of EML4-ALK oncokinase for the growth/survival of not only primary tumors but of the metastases. Such profound effects were rare among the patients when treated with conventional cytotoxic anticancer drugs.

The three cases which were enrolled for the study had surprisingly similar biological characteristics. They had multiple bone and lymph node metastases at the first medical examination, and were non-smokers at younger ages (48–54) who were resistant to chemotherapy. Adverse effects with crizotinib were also similar among them, including transient diarrhea, nausea, light image persistence, and subjective changes of taste. In addition, their response to ALK inhibitor was similar. Bone and lymph node metastases had disappeared within one month after the initiation of the therapy. The response of the primary tumor in case 2 was relatively slow compared with those of the metastases. The difference between the response of primary tumor and metastases to the ALK inhibitor in this case seems to indicate that the similar subclones of tumor cells in the primary tumors that were highly responsive to ALK inhibitor metastasized to distant organs and may give some explanation for the discrepancy in the time-course between CEA and CA125.

Molecular and immunohistochemical analyses in this cohort were conducted on the basis of the specimens obtained through EBUS-TBNA. Originally, EBUS-TBNA had been proposed useful for the pathological diagnosis of mediastinal involvement (N2 disease) of lung cancer [17–20]. However, we have already reported that EBUS-TBNA is also a versatile way of obtaining histological samples for the molecular analyses of cancer-related genes, such as *EGFR*, p53 et al. [21,22]. For those who have advanced NSCLC, it is often difficult to conduct surgery to obtain specimens from patients. Among such cases, however, EBUS-TBNA can usually be safely carried out to obtain specimens from enlarged mediastinal

lymph nodes or parathracheal tumors. We carried out EBUS-TBNA procedure for the reasons of its advantage in obtaining high quality core samples adequate for this purpose as well as its safety. We do not disregard the importance of TBB for the diagnosis of lung cancer; however, we needed histological samples to examine the immunohistochemistry and FISH for enrolment in a trial of crizotinib. Our experience with the three cases clearly demonstrates the importance and clinical relevance of obtaining such specimens for molecular analyses.

Although the initial effects of crizotinib are substantial in our cases, as well as in those reported by Bang et al. [10,11], such efficacy may not always last long. There was, for instance, development (case 1 and 2) and recurrence (case 3) of brain metastases while favorable control was maintained outside the brain. Given that the primary tumors and lymph node metastases were under control of crizotinib even at the appearance of brain metastases, the tumor cells outside the brain did not lose sensitivity to crizotinib. Relapses in the brain only may indicate either (i) subclones of the tumor acquired both the homing ability to the brain and resistance to crizotinib, or (ii) crizotinib may not penetrate the blood-brain barrier, leading to insufficient concentrations of crizotinib in the brain. It is thus highly important to examine in detail the molecular basis that would account for such acquired resistance to crizotinib, which may be secondary mutations within EML4-ALK itself or mutations/gene amplification of other genes, as demonstrated in the cases of acquired resistance of NSCLC to gefitinib/erlotinib [23–26].

Conflict of interest

None declared.

Acknowledgements

We are grateful to Dr. Yung-Jue Bang and the medical staff of Seoul National University Hospital for their support in the treatment of these patients. We also thank Mr. C.W.P. Reynolds of the Department of International Medical Communications, Tokyo Medical University, for his careful revision of the English of this manuscript.

References

[1] Janku F, Stewart DJ, Kurzrock R. Targeted therapy in non-small-cell lung cancer—Is it becoming a reality? Nat Rev Clin Oncol 2010 Jun 15;7(July (7)):401–14.
[2] Heinrich MC, Owzar K, Corless CL, et al. Correlation of kinase genotype and clinical outcome in the North American intergroup phase III trial of imatinib mesylate for treatment of advanced gastrointestinal stromal tumor: CALGB 150105 study by cancer and leukemia group B and southwest oncology group. J Clin Oncol 2008;26:5360–7.
[3] Mok TS, Wu YL, Yu CJ, et al. Randomized, placebo-controlled, phase II study of sequential erlotinib and chemotherapy as first-line treatment for advanced non-small-cell lung cancer. J Clin Oncol 2009;27:5080–7.
[4] Soda M, Choi YL, Enomoto M, et al. Identification of the transforming EML4-ALK fusion gene in non-small-cell lung cancer. Nature 2007;448:561–6.
[5] Mano H. Non-solid oncogenes in solid tumors: EML4-ALK fusion genes in lung cancer. Cancer Sci 2008;99:2349–55.
[6] Soda M, Takada S, Takeuchi K, et al. A mouse model for EML4-ALK-positive lung cancer. Proc Natl Acad Sci USA 2008;105:19893–7.
[7] Christensen JG, Zou HY, Arango ME, et al. Cytoreductive antitumor activity of PF-2341066, a novel inhibitor of anaplastic lymphoma kinase and c-Met, in experimental models of anaplastic large-cell lymphoma. Mol Cancer Ther 2007;6:3314–22.
[8] Koivunen JP, Mermel C, Zejnullahu K, et al. EML4-ALK fusion gene and efficacy of an ALK kinase inhibitor in lung cancer. Clin Cancer Res 2008;14: 4275–83.
[9] Kwak EL, Camidge DR, Clark J, et al. Clinical activity observed in a phase I dose escalation trial of an oral c-met and ALK inhibitor, PF-02341066. J Clin Oncol 2009;27:15s.
[10] Bang Y, Kwak EL, Shaw AT, et al. Clinical activity of the oral ALK inhibitor PF-02341066 in ALK-positive patients with non-small cell lung cancer (NSCLC). J Clin Oncol 2010;28:18s [suppl; abstr 3].
[11] Kwak EL, Bang YJ, Camidge DR, et al. Anaplastic lymphoma kinase inhibition in non-small-cell lung cancer. N Engl J Med 2010;363:1693–703.
[12] Takeuchi K, Choi YL, Togashi Y, et al. KIF5B-ALK, a novel fusion oncokinase identified by an immunohistochemistry-based diagnostic system for ALK-positive lung cancer. Clin Cancer Res 2009;15:3143–9.
[13] Inamura K, Takeuchi K, Togashi Y, et al. EML4-ALK lung cancers are characterized by rare other mutations, a TTF-1 cell lineage, an acinar histology, and young onset. Mod Pathol 2009;22:508–15.
[14] Shaw AT, Yeap BY, Mino-Kenudson M, et al. Clinical features and outcome of patients with non-small-cell lung cancer who harbor EML4-ALK. J Clin Oncol 2009;27(September (26)):4247–53.
[15] Takahashi T, Snooze M, Kobayashi M, et al. Clinicopathologic features of non-small-cell lung cancer with EML4-ALK fusion gene. Ann Surg Oncol 2010;17(March (3)):889–97.
[16] Nakajima T, Kimura H, Takeuchi K, et al. Treatment of lung cancer with an ALK inhibitor after EML4-ALK fusion gene detection using endobronchial ultrasound-guided transbronchial needle aspiration. J Thorac Oncol 2010;5:2041–3.
[17] Yasufuku K, Chiyo M, Koh E, et al. Endobronchial ultrasound guided transbronchial needle aspiration for staging of lung cancer. Lung Cancer 2005;50:347–54.
[18] Yasufuku K, Chiyo M, Sekine Y, et al. Real-time endobronchial ultrasound-guided transbronchial needle aspiration of mediastinal and hilar lymph nodes. Chest 2004;126:122–8.
[19] Herth FJ, Eberhardt R, Vilmann P, Krasnik M, Ernst A. Real-time endobronchial ultrasound guided transbronchial needle aspiration for sampling mediastinal lymph nodes. Thorax 2006;61:795–8.
[20] Herth FJ, Ernst A, Eberhardt R, Vilmann P, Dienemann H, Krasnik M. Endobronchial ultrasound-guided transbronchial needle aspiration of lymph nodes in the radiologically normal mediastinum. Eur Respir J 2006;28: 910–4.
[21] Nakajima T, Yasufuku K, Suzuki M, et al. Assessment of epidermal growth factor receptor mutation by endobronchial ultrasound-guided transbronchial needle aspiration. Chest 2007;132:597–602.
[22] Mohamed S, Yasufuku K, Nakajima T, et al. Analysis of cell cycle-related proteins in mediastinal lymph nodes of patients with N2-NSCLC obtained by EBUS-TBNA: relevance to chemotherapy response. Thorax 2008;63:642–7.
[23] Kobayashi S, Boggon TJ, Dayaram T, et al. EGFR mutation and resistance of non-small-cell lung cancer to gefitinib. N Engl J Med 2005;352:786–92.
[24] Lu L, Ghose AK, Quail MR, et al. ALK mutants in the kinase domain exhibit altered kinase activity and differential sensitivity to small molecule ALK inhibitors. Biochemistry 2009;48:3600–9.
[25] Gazdar AF. Activating and resistance mutations of *EGFR* in non-small-cell lung cancer: role in clinical response to EGFR tyrosine kinase inhibitors. Oncogene 2009;28:S24–31.
[26] Choi YL, Soda M, Yamashita Y, et al. EML4-ALK mutations in lung cancer that confer resistance to ALK inhibitors. N Engl J Med 2010;363:1734–9.

OPEN ACCESS Freely available online

PLoS one

Ex Vivo Expansion of Human CD8$^+$ T Cells Using Autologous CD4$^+$ T Cell Help

Marcus O. Butler[1,2,3], Osamu Imataki[1,2,3], Yoshihiro Yamashita[4], Makito Tanaka[1,2,3], Sascha Ansén[1,2,3], Alla Berezovskaya[1], Genita Metzler[1], Matthew I. Milstein[1], Mary M. Mooney[1], Andrew P. Murray[1], Hiroyuki Mano[4,5], Lee M. Nadler[1,2,3], Naoto Hirano[1,2,3,6,7]*

1 Department of Medical Oncology, Dana-Farber Cancer Institute, Massachusetts, United States of America, **2** Department of Medicine, Brigham and Women's Hospital, Massachusetts, United States of America, **3** Department of Medicine, Harvard Medical School, Boston, Massachusetts, United States of America, **4** Division of Functional Genomics, Jichi Medical University, Tochigi, Japan, **5** Department of Medical Genomics, University of Tokyo, Tokyo, Japan, **6** Immune Therapy Program, Campbell Family Institute for Breast Cancer Research, Campbell Family Cancer Research, Ontario Cancer Institute, Toronto, Ontario, Canada, **7** Department of Immunology, University of Toronto, Toronto, Ontario, Canada

Abstract

Background: Using *in vivo* mouse models, the mechanisms of CD4$^+$ T cell help have been intensively investigated. However, a mechanistic analysis of human CD4$^+$ T cell help is largely lacking. Our goal was to elucidate the mechanisms of human CD4$^+$ T cell help of CD8$^+$ T cell proliferation using a novel *in vitro* model .

Methods/Principal Findings: We developed a genetically engineered novel human cell-based artificial APC, aAPC/mOKT3, which expresses a membranous form of the anti-CD3 monoclonal antibody OKT3 as well as other immune accessory molecules. Without requiring the addition of allogeneic feeder cells, aAPC/mOKT3 enabled the expansion of both peripheral and tumor-infiltrating T cells, regardless of HLA-restriction. Stimulation with aAPC/mOKT3 did not expand Foxp3$^+$ regulatory T cells, and expanded tumor infiltrating lymphocytes predominantly secreted Th1-type cytokines, interferon-γ and IL-2. In this aAPC-based system, the presence of autologous CD4$^+$ T cells was associated with significantly improved CD8$^+$ T cell expansion *in vitro*. The CD4$^+$ T cell derived cytokines IL-2 and IL-21 were necessary but not sufficient for this effect. However, CD4$^+$ T cell help of CD8$^+$ T cell proliferation was partially recapitulated by both adding IL-2/IL-21 and by upregulation of IL-21 receptor on CD8$^+$ T cells.

Conclusions: We have developed an *in vitro* model that advances our understanding of the immunobiology of human CD4$^+$ T cell help of CD8$^+$ T cells. Our data suggests that human CD4$^+$ T cell help can be leveraged to expand CD8$^+$ T cells *in vitro*.

Citation: Butler MO, Imataki O, Yamashita Y, Tanaka M, Ansén S, et al. (2012) Ex Vivo Expansion of Human CD8$^+$ T Cells Using Autologous CD4$^+$ T Cell Help. PLoS ONE 7(1): e30229. doi:10.1371/journal.pone.0030229

Editor: Derya Unutmaz, New York University, United States of America

Received April 7, 2011; **Accepted** December 13, 2011; **Published** January 12, 2012

Funding: This work was supported by the Madeleine Franchi Ovarian Research Fund (MOB), Dunkin Donuts Rising Stars Awards (MOB and NH), a grant from the Cancer Research Institute (LMN), NIH grant K22 CA129240 (NH), NIH grant R01 CA148673 (NH), and the American Society of Hematology Scholar Award (NH). The funders had no role in study design, data collection and analysis, decision to publish, or preparation of the manuscript.

Competing Interests: MOB, LMN and NH have filed a patent application related to aAPC/A2. The patent application number is 10/850,294 and is entitled, "Modified Antigen-Presenting Cells." The authors confirm that this application does not alter their adherence to all PLoS ONE policies on the sharing of data and materials.

* E-mail: nhirano@uhnres.utoronto.ca

Introduction

It is now well accepted that neoplastic cells are immunogenic and that tumors develop in the context of immune recognition by the host [1,2]. Tumor-associated antigens that serve as immune targets include cell lineage differentiation antigens, cancer-testes antigens, and neoantigens produced by mutations in the cancer cell's unstable genome. Mutational events can give rise to multiple immunogenic MHC class I and II restricted, non-self epitopes capable of inducing strong immune responses to the tumor [3,4]. In several maligancies, anti-tumor T cell responses, with infiltration of tumors by CD8$^+$ T lymphocytes and local production of interferon-γ and IL-2, have been associated with improved clinical prognosis [5–8].

Counter regulatory immune responses, however, also develop in the cancer-bearing host. Tumors subvert the immune response by secreting chemotactic factors that recruit immune suppressive elements, thereby inhibiting the function of anti-tumor effectors [9]. Tumor infiltration by T regulatory (Treg) cells has been correlated with inferior clinical outcomes in several tumors [10,11]. These findings have led to the proposal that immune recognition of cancer involves the balancing of opposing forces: anti-tumor effectors vs. pro-tumor regulatory elements [10,12,13]. In fact, a high ratio of Treg cells to CD8$^+$ T cells within the tumor microenvironment has been associated with poorer survival [14,15].

Adoptive T cell therapy is a promising treatment modality designed to amplify the anti-tumor immune response. Anti-tumor effectors are expanded *in vitro*, away from the pro-tumor milieu of the cancer bearing host, and then reinfused as a cellular therapy [16–21]. Successful approaches showing clinical activity include adoptive transfer of tumor antigen-specific T cell lines or clones

that have been derived from the peripheral blood. Specificity can be achieved by stimulating antigen-specific precursor T cells or through genetic modification of expanded bulk T cells to express cloned or chimeric T cell receptor (TCR) genes [22–26]. Alternatively, the nascent, endogenous immune effector response to the tumor can be amplified by expanding tumor-infiltrating lymphocytes (TIL) *in vitro*. Adoptive cell transfer of *in vitro* activated TIL has achieved major clinical responses when patients first undergo lymphodepletion and are then given high dose IL-2 after adoptive transfer [17,27]. Lymphodepletion augments the persistence and function of transferred TIL not only by reducing or temporarily eliminating Treg cells, but also by reducing cytokine sinks that results in the accumulation of homeostatic cytokines such as IL-7 and IL-15 [28,29].

The optimal method for generating clinically effective T cell grafts *in vitro* has yet to be established [21,30]. In order to achieve massive numerical expansion of T cells, current methods necessitate the use of soluble monoclonal antibodies (mAb), allogeneic feeder PBMC, EBV transformed lymphoblastoid cell lines, and/or undefined culture supernatants. Consequently, these requirements present formidable challenges and costs that prevent the widespread clinical application of this therapy. While adoptive transfer of anti-tumor $CD4^+$ T cells can be efficacious, expansion of anti-tumor $CD8^+$ T cells is also an important goal, particularly in light of the association between their persistence and clinical responses [18,31–33].

Insights into requirements for augmenting the expansion of both $CD4^+$ and $CD8^+$ T cells will help further improve methods to generate T cell grafts for adoptive therapy. $CD4^+$ T cells help generate effective immune responses by sustaining $CD8^+$ T cell proliferation, preventing exhaustion, and establishing long-lived functional memory [34]. In mouse models, common γ-chain receptor cytokine and CD40 signaling can mediate $CD4^+$ T cell help [34–44]. In clinical studies, $CD4^+$ T cells have also been implicated in promoting the persistence and anti-tumor activity of antigen-specific $CD8^+$ T cells in patients [45,46]. However, the mechanisms of human $CD4^+$ T cell help are less well understood. To conduct a mechanistic analysis of human $CD4^+$ T cell help, we developed a novel, human cell-based aAPC, aAPC/mOKT3, which induces both $CD4^+$ and $CD8^+$ T cell expansion without allogeneic feeder cells. The removal of allogeneic feeder cells from our T cell culture system enabled us to precisely isolate molecules mediating help of $CD8^+$ T cell expansion that are expressed or secreted by human $CD4^+$ T cells.

Results

K562-based aAPC expressing membranous OKT3 induces $CD3^+$ T cell expansion

We and others have previously reported the generation of aAPC derived from the human erythroleukemia cell line K562 [47–51]. K562 serves as an excellent platform for generating aAPC since it expresses no HLA class I or II molecules, but highly expresses adhesion molecules such as CD54 and CD58. Using K562, we developed a novel aAPC, aAPC/mOKT3, capable of expanding $CD3^+$ T cells regardless of HLA subtype (Figure 1A, Figure S1). This aAPC was engineered to express a membranous form of the anti-CD3 mAb, OKT3, on its cell surface, thus obviating the need for adding soluble mAb to T cell cultures or loading it onto aAPC as described elsewhere [51,52]. aAPC/mOKT3 also ectopically expresses immunostimulatory molecules CD80 and CD83. We and others have shown that CD83 delivers a CD80 dependent signal that promotes lymphocyte longevity [47,53,54].

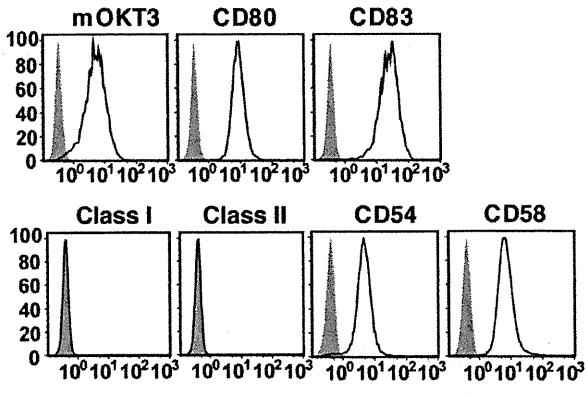

Figure 1. Generation of aAPC/mOKT3. Surface expression of a transduced membranous form of anti-CD3 mAb, and transduced CD80, CD83, and endogenous HLA class I, class II, CD54, and CD58 on aAPC/mOKT3 is shown. A membranous form of anti-CD3 mAb on aAPC/mOKT3 (open) and wild type K562 (shaded) was stained using goat anti-mouse IgG (H+L). Other surface molecules were stained with each specific mAb (open) and isotype control (shaded) and analyzed by flow cytometry. Note the lack of endogenous expression of HLA class I and II on aAPC/mOKT3.
doi:10.1371/journal.pone.0030229.g001

Stimulation of $CD3^+$ T cells with aAPC/mOKT3 induces robust $CD8^+$ T cell expansion

Peripheral $CD3^+$ T cells expanded with aAPC/mOKT3 were phenotypically characterized after 28 days in culture (Figure 2). While the number of both $CD4^+$ and $CD8^+$ T cells increased, $CD8^+$ T cells expanded substantially better than $CD4^+$ T cells, and therefore dominated cultures from every donor tested (Figure 2A). This is in contrast to other pan T cell expansion systems such as anti-CD3/CD28 mAb-coated beads, which invariably favor the expansion $CD4^+$ T cells over $CD8^+$ T cells [55] (Figure 2B). Similar fold expansion of $CD3^+$ T cells was obtained with the aAPC/mOKT3-based and antibody-coated bead-based expansion systems. T cells expanded using aAPC/mOKT3 displayed a central memory~effector memory phenotype ($CD45RA^-$ $CD54RO^+$ $CD62L^{+/-}$) and retained expression of receptors for IL-2, IL-7, and IL-21 (Figure 2C). CD40 ligand was highly expressed by $CD4^+$ T cells but not $CD8^+$ T cells. Importantly, expanded $CD4^+$ $CD25^+$ T cells did not express Foxp3, indicating that immunoinhibitory Treg cells did not proliferate well (Figure 2D).

aAPC/mOKT3 induces unbiased $CD3^+$ T cell expansion, preserving the repertoire for viral and tumor-associated antigens

In order to evaluate whether stimulation with aAPC/mOKT3 induced broad expansion of $CD3^+$ T cells, TCR Vβ repertoire analysis was performed. No obvious skewing in the TCR Vβ usage of both $CD4^+$ and $CD8^+$ T cell populations was revealed, supporting "unbiased" T cell expansion by aAPC/mOKT3 (Figure 3A). Moreover, HLA-restricted antigen-specific $CD8^+$ cytotoxic T lymphocytes (CTL) against viral and tumor antigens could be generated from $CD3^+$ T cells initially expanded for four weeks using aAPC/mOKT3 (Figure 3B and 3C). The functional avidity of these tumor antigen-specific T cells was sufficient to recognize tumor targets endogenously expressing antigen, confirming that the T cell repertoire for tumor antigen recognition was preserved (Figure 3C). We also confirmed that stimulation with aAPC/mOKT3 induced the expansion of tumor-antigen specific T cells. After 28 days in culture, MART1 peptide specific $CD8^+$ T cell expansion was 420–1,150 fold (Figure S1D).

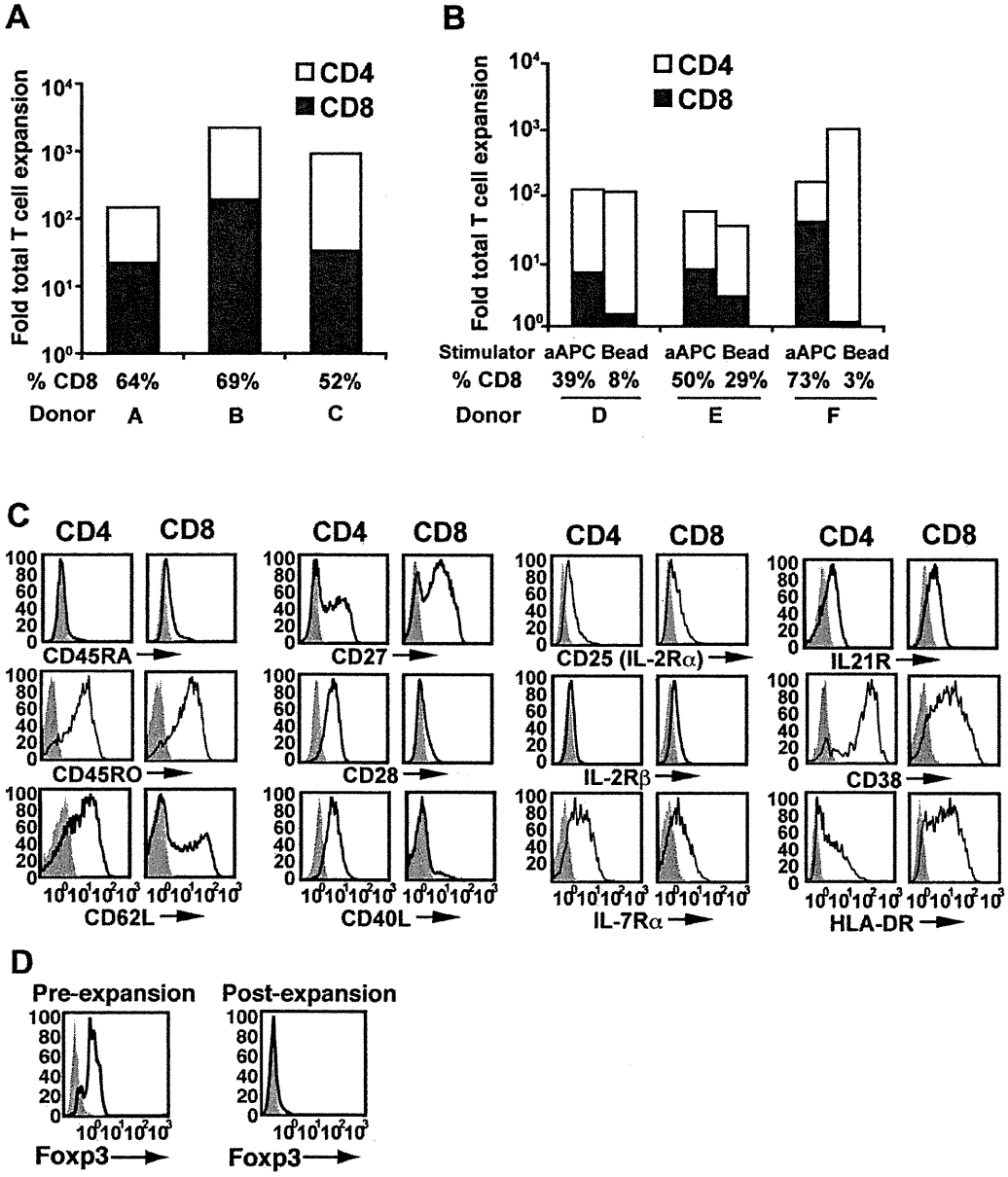

Figure 2. aAPC/mOKT3 expands both CD4+ and CD8+ T cells without using allogeneic feeder PBMC. (**A**) CD3+ T cells were stimulated twice with aAPC/mOKT3 and supplemented with IL-2 between stimulations. Fold expansion of CD3+ T cells over one month is shown for three donors. Shading shows the proportion of expanded CD4+ (white) and CD8+ (black) T cells, and percent CD8+ T cells is indicated. (**B**) CD3+ T cells were stimulated twice with aAPC/mOKT3 or beads (Dynabeads CD3/CD28) and supplemented with IL-2 between stimulations. Fold expansion of CD3+ T cells over one month is shown for three donors. Shading shows the proportion of expanded CD4+ (white) and CD8+ (black) T cells, and percent CD8+ T cells is indicated. (**C**) CD3+ T cells were expanded as described in Figure 2A. Expression of surface molecules on gated CD4+ and CD8+ T cells is shown (open). Isotype mAb staining was used as a control (shaded). (**D**) CD4+ CD25+ Foxp3+ Treg cells, present pre-expansion, were absent in expanded cultures. CD4+ CD25+ cells, pre- and post-expansion, were stained intracellularly with anti-Foxp3 mAb (open) and isotype control (shaded).
doi:10.1371/journal.pone.0030229.g002

aAPC/mOKT3 expands functional TIL but not contaminating Treg cells

Using aAPC/mOKT3, lymphocytes derived from malignant ascites (breast and ovarian cancer) and melanoma metastases were successfully expanded without adding any allogeneic feeder cells (Figure 4A). As observed with peripheral CD3+ T cells in Figure 2A, CD8+ T cells predominantly expanded in all cultures, including those that initially contained a minimal percentage of CD8+ T cells. Importantly, Foxp3+ cells did not proliferate well (Figure 4B). As with peripheral CD3+ T cells, expanded TIL had a central memory~effector memory phenotype (CD45RA- CD62L+/-) consistent with a lack of terminal differentiation (Figure S2). Furthermore, expanded T cells highly expressed CD27 and CD28 which are associated

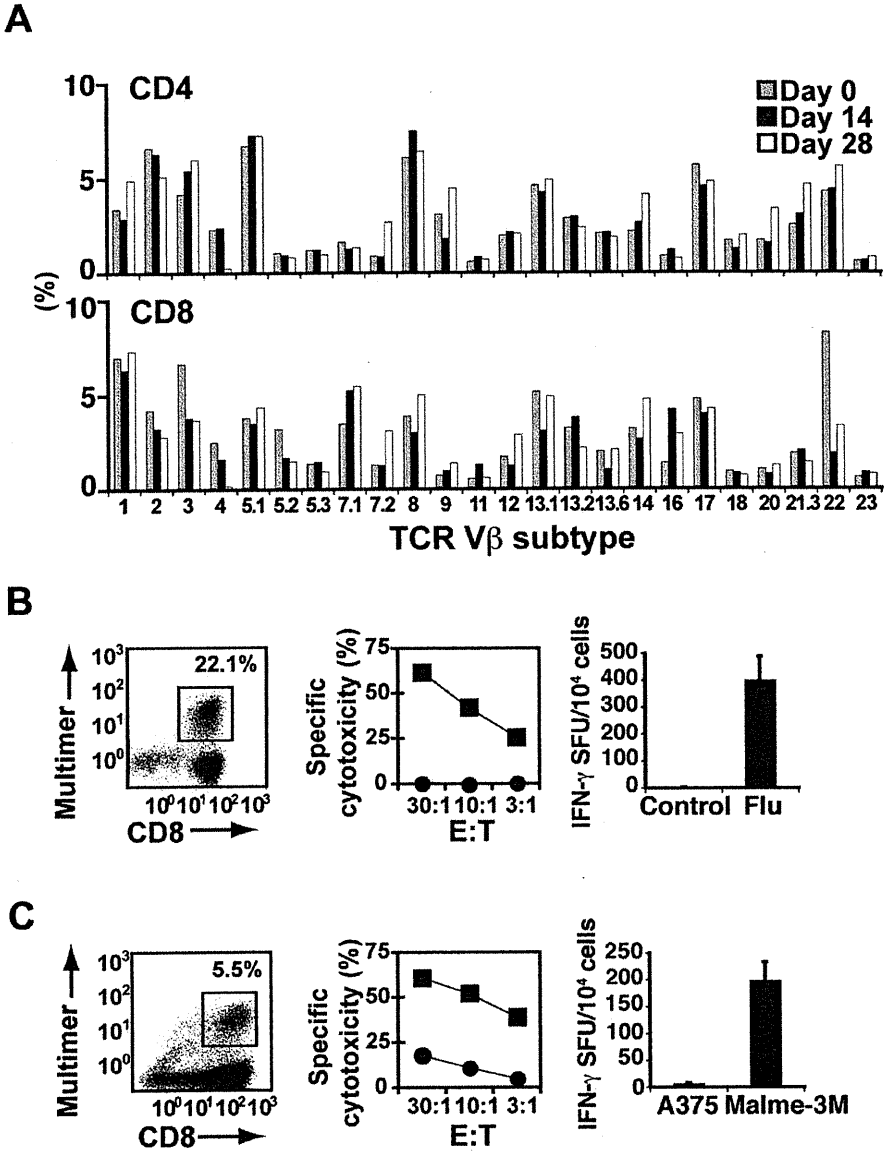

Figure 3. Expansion with aAPC/mOKT3 does not induce skewing of the TCR Vβ repertoire. (**A**) TCR Vβ subfamily analysis before and after stimulation with aAPC/mOKT3 is shown. $CD3^+$ T cells were stimulated with aAPC/mOKT3 on days 0 and 14 and were treated with IL-2 at 300 IU/ml between stimulations. TCR Vβ usage analysis was performed on days 0, 14, 28. Data shown is on gated $CD4^+$ and $CD8^+$ T cells. (**B, C**) $A2^+$ $CD3^+$ T cells were stimulated twice with aAPC/mOKT3 for one month. Subsequently, $CD8^+$ T cells were purified from expanded $CD3^+$ T cells and further stimulated with aAPC/A2 pulsed with Flu or MART1 peptide. (**B**) Flu specificity was demonstrated by multimer staining (left). Functional competence was demonstrated by antigen-specific cytotoxicity (middle) and IFN-γ secretion (right). T2 cells pulsed with Flu peptide (■) or control peptide (●) were used as targets. (**C**) MART1 specificity was similarly demonstrated by multimer staining (left). The HLA-$A2^+$/$MART1^+$ melanoma line, Malme-3M (■), and the HLA-$A2^+$/$MART1^-$ melanoma line, A375 (●), were used as targets in cytotoxicity (middle) and IFN-γ ELISPOT assays (right).
doi:10.1371/journal.pone.0030229.g003

with T cell survival and persistence *in vivo* [56-59]. They also secreted high quantities of IFN-γ and IL-2, while IL-4 secretion was lower and no IL-10 was produced (Figure 4C). These results demonstrate that the aAPC/mOKT3-based system can expand tumor-infiltrating $CD8^+$ T cells in the presence of autologous $CD4^+$ T cells, and that they display phenotypic and functional characteristics consistent with central memory~effector memory T cells.

IL-2 and IL-21 are necessary, but not sufficient, for $CD4^+$ T cell-mediated help of $CD8^+$ T cell expansion

Using the aAPC/mOKT3-based expansion system, we compared the expansion of $CD8^+$ T cells in the presence or absence of $CD4^+$ T cells. $CD8^+$ T cells expanded much better in the presence of $CD4^+$ T cells (Figure 5A), suggesting the presence of $CD4^+$ T cell help for $CD8^+$ T cells in these aAPC/mOKT3-based cultures. We tested whether this "help" was mediated by soluble factors or

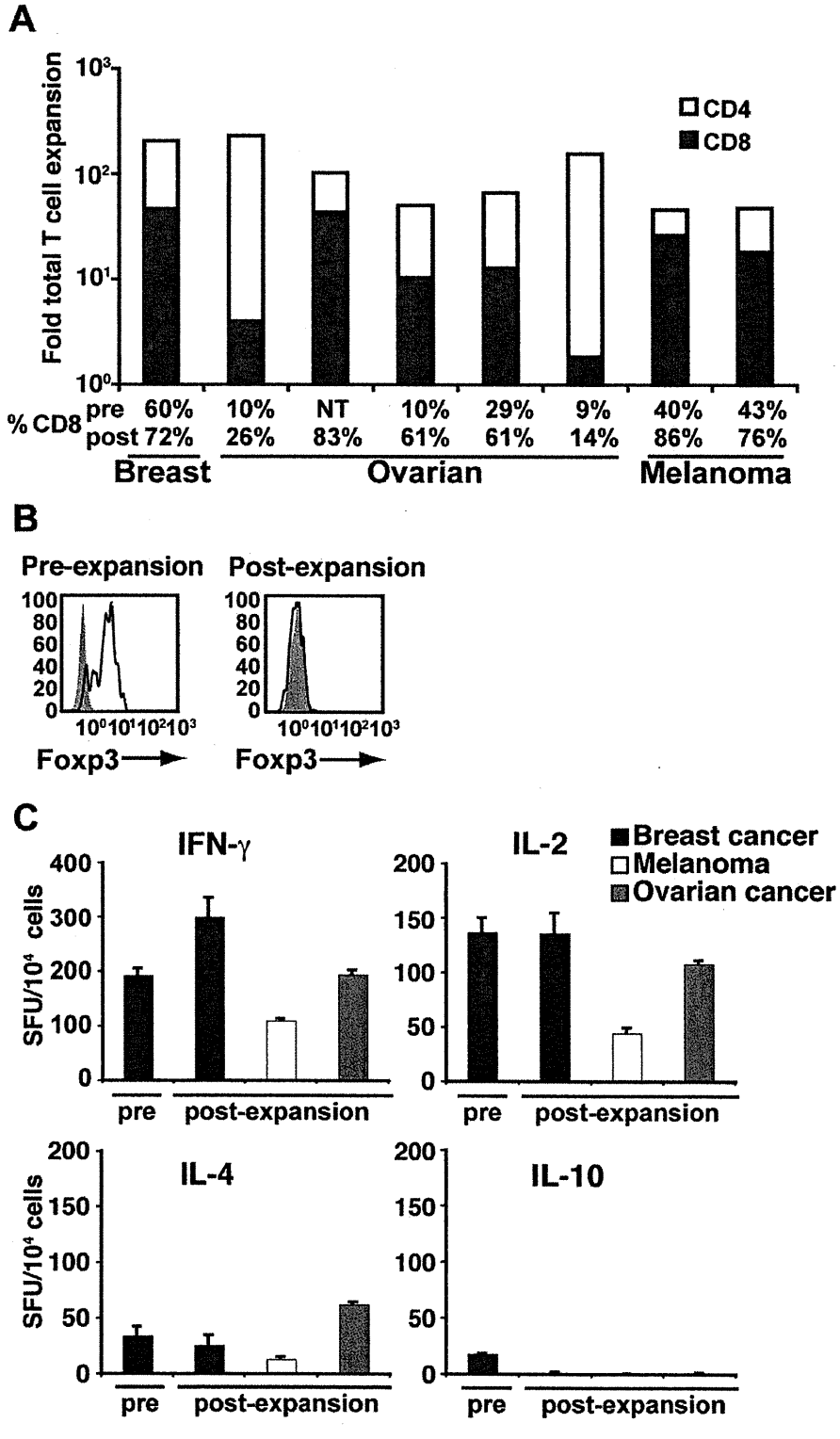

Figure 4. aAPC/mOKT3 expanded TIL are Foxp3 negative and secrete predominantly Th1 cytokines. (**A**) Expansion of TIL obtained from breast and ovarian cancer ascites and melanoma metastases is shown. Shading indicates the proportion of $CD4^+$ (white) and $CD8^+$ (black) T cells in expanded cultures. The percentage of $CD8^+$ T cells in pre- and post-expansion cultures is shown. Note that in all samples tested, the percentage of $CD8^+$ T cells increased even in those that initially contained a minimal percentage of $CD8^+$ T cells. NT denotes not tested. (**B**) $CD4^+$ $CD25^+$ $Foxp3^+$ Treg